

Nonequilibrium Quasiparticle Distribution in Superconducting Resonators: An Analytical Approach

P.B. Fischer^{1,2} and G. Catelani^{1,3,*}

¹*JARA Institute for Quantum Information (PGI-11), Forschungszentrum Jülich, 52425 Jülich, Germany*

²*JARA Institute for Quantum Information, RWTH Aachen University, 52056 Aachen, Germany*

³*Quantum Research Center, Technology Innovation Institute, P.O. Box 9639, Abu Dhabi, United Arab Emirates*



(Received 15 December 2022; revised 13 March 2023; accepted 28 April 2023; published 26 May 2023)

In the superconducting state, the presence of a finite gap in the excitation spectrum implies that the number of excitations (quasiparticles) is exponentially small at temperatures well below the critical temperature. Conversely, minute perturbations can significantly impact both the distribution in energy and the number of quasiparticles. Typically, the interaction with the electromagnetic environment is the main perturbation source driving quasiparticles out of thermal equilibrium, while a phonon bath is responsible for restoration of equilibrium. Here we derive approximate analytical solutions for the quasiparticle distribution function in superconducting resonators and explore the impact of nonequilibrium on two measurable quantities: the resonator's quality factor and its resonance frequency. Applying our results to experimental data, we conclude that while at intermediate temperatures there is clear evidence for the nonequilibrium effects due to heating of the quasiparticles by photons, the low-temperature measurements are not explained by this mechanism.

DOI: [10.1103/PhysRevApplied.19.054087](https://doi.org/10.1103/PhysRevApplied.19.054087)

I. INTRODUCTION

Nonequilibrium effects in superconductors have long attracted the interest of both experimentalists and theorists, starting with observations in the 1960s of enhancements in the critical current of weak links subjected to microwaves [1,2]. Soon after, theoretical work [3] predicted enhancements not only of the critical current but also of the critical temperature T_c and the gap Δ (see Ref. [4] for an early review and Ref. [5] for a recent one). These effects are generally related to a redistribution in energy of quasiparticles: in a superconductor, the density of states is lower at higher energy, so a given number of quasiparticle excitations is less harmful to superconductivity if they are shifted to higher energy by the microwaves. The effects are more evident near T_c , where they were initially discovered, but more recently the focus has shifted to temperatures low compared with T_c , where nonequilibrium quasiparticles can be a resource or a complication. They are a resource in detectors such as kinetic inductance [6] and nanowire single-photon detectors [7], while they negatively affect qubits, electron pumps and turnstiles, and microrefrigerators [8]. A fundamental question that we address here is how the quasiparticles redistribute themselves in energy at low temperature $T \ll T_c$. The theoretical model to study this question can be written in the

form of a kinetic equation for the quasiparticle distribution function in the presence of the microwave drive and accounting for the interaction with phonons, whose distribution is also determined by a kinetic equation [9]. Solving for the distribution function in the presence of microwaves is, in general, challenging, since the full model consists of coupled nonlinear integral equations. Assuming $T = 0$, some basic properties of the solution were considered in Ref. [10]; recently, a more-detailed analysis of this case, where linearization is possible, was given in Ref. [11]. The main qualitative result of that work is the identification of two regimes, cold and hot quasiparticles: cold quasiparticles have energy largely close to the gap, while hot ones are more broadly distributed over an energy T_* that depends on the strength of the microwave drive; the latter determines the transition between the two regimes. The assumption $T = 0$ means that the phonon distribution is fixed to be zero; to our knowledge, the full model allowing for nonequilibrium phonons has been studied only numerically [12]. Here we build on the results in Ref. [11] to arrive at an analytical description of the hot-quasiparticle case beyond the linearized regime. This description, in turn, enables us to derive explicit formulas for the internal quality factor of superconducting resonators that can be compared with experimental measurements. Our main finding is that the energy scale T_*^2/Δ^2 separates two qualitatively different regimes: for phonon temperature above this scale, the quasiparticle density is close to its

*g.catelani@fz-juelich.de

thermal value and the quality factor decreases exponentially with temperature and increases with drive strength; vice versa, for temperature below this scale, the density is much higher than the thermal value and the quality factor depends weakly on temperature and decreases with drive strength. For temperatures above T_*^3/Δ^2 , our results agree quantitatively with the measurements reported in Ref. [13].

Although the focus of this article is on the nonequilibrium quasiparticle distribution, our results are relevant to applications such as kinetic inductance detectors. For example, the existence of two different regimes depending on temperature and microwave drive strength could impact the way the detectors are characterized and their response is calibrated [14]. This work can also enable further research on the impact of material parameters on the detector responsivity; see, for instance, Ref. [15]. More broadly, understanding the effects of phonons and photons on the quasiparticle distribution in resonators can provide a reference point in the study of other superconducting systems, such as nanobridge junctions [16] and granular superconductors [17].

In the next section we briefly review the kinetic equations for quasiparticles and phonons to establish our notation. In Sec. III we first extend the $T = 0$ solution for the quasiparticle distribution to a wider energy range than that in Ref. [11]; then we consider finite phonon temperature as well as deviations of the phonon distribution from its equilibrium form. Going beyond the linearized model, we consider in Sec. IV the effect of microwave photons on quasiparticle density and the superconducting gap; the analytical results are validated by comparison with numerical solutions. Section V presents the calculation of the quality factor and the resonance frequency, as well as comparison with experiments. We summarize our work in Sec. VI.

II. KINETIC EQUATIONS

The quasiparticle distribution function $f(E)$ in a superconductor obeys the kinetic equation

$$\frac{df(E)}{dt} = \text{St}^{\text{phon}}\{f, n\} + \text{St}^{\text{phot}}\{f, \bar{n}\}, \quad (1)$$

with the two collision integrals $\text{St}^{\text{phon}}\{f, n\}$ and $\text{St}^{\text{phot}}\{f, \bar{n}\}$ accounting for the interaction of quasiparticles with phonons and photons, respectively. In our notation, $n(\omega)$ represents the distribution function of phonons and \bar{n} represents the (average) number of photons. The collision integrals can be derived with use of nonequilibrium Green's functions [18] or Fermi's golden rule [19], and can be generally split into terms that conserve or change the number of quasiparticles. Note that we assume the system to be homogeneous, so the distribution functions are independent of position. The kinetic equation is complemented by

the self-consistent equation for the superconducting gap Δ :

$$\ln\left(\frac{\Delta_0}{\Delta}\right) = \int_{\Delta}^{\infty} dE \rho(E) \frac{2f(E)}{E}, \quad (2)$$

where Δ_0 is the zero-temperature gap (i.e., in the absence of quasiparticles) and

$$\rho(E) = \frac{E}{\sqrt{E^2 - \Delta^2}} \quad (3)$$

is the normalized density of states.

A. Interaction with phonons

For the phonon collision integral, in the term conserving the quasiparticle number we distinguish spontaneous emission of phonons from stimulated emission and absorption, while the number-nonconserving terms account for recombination of quasiparticles into Cooper pairs and pair-breaking events:

$$\begin{aligned} \text{St}^{\text{phon}}\{f, n\} = & \text{St}_{\text{sp}}^{\text{phon}}\{f\} + \text{St}_{\text{st}}^{\text{phon}}\{f, n\} + \text{St}_r^{\text{phon}}\{f, n\} \\ & + \text{St}_{\text{PB}}^{\text{phon}}\{f, n\}. \end{aligned} \quad (4)$$

The first term on the right-hand side describes spontaneous emission (we use units with $k_B = \hbar = 1$):

$$\begin{aligned} \text{St}_{\text{sp}}^{\text{phon}}\{f\} = & \frac{1}{\tau_0 T_c^3} \left\{ \int_0^{\infty} d\omega \omega^2 U^-(E, E + \omega) f(E + \omega) [1 - f(E)] \right. \\ & \left. - \int_0^{E-\Delta} d\omega \omega^2 U^-(E, E - \omega) f(E) [1 - f(E - \omega)] \right\}, \end{aligned} \quad (5)$$

where $T_c \simeq \Delta_0/1.764$ is the critical temperature and the functions

$$U^{\pm}(E, E') = \rho(E') K^{\pm}(E, E') \quad (6)$$

are given by a product between the density of states, Eq. (3), and the BCS coherence factors [20]

$$K^{\pm}(E, E') = 1 \pm \frac{\Delta^2}{EE'}. \quad (7)$$

Finally, the factor $\omega^2/T_c^3\tau_0$ accounts for the strength of the electron-phonon interaction in the Debye model and in a low-frequency approximation appropriate for weakly coupled superconductors [21].

With the notation introduced above, the contribution of stimulated emission and absorption is given by

$$\begin{aligned} \text{St}_{\text{st}}^{\text{phon}}\{f, n\} &= \frac{1}{\tau_0 T_c^3} \int_0^\infty d\omega \omega^2 U^-(E, E + \omega) \{f(E + \omega) [1 - f(E)] - f(E) [1 - f(E + \omega)]\} n(\omega) \\ &+ \frac{1}{\tau_0 T_c^3} \int_0^{E-\Delta} d\omega \omega^2 U^-(E, E - \omega) \{f(E - \omega) [1 - f(E)] - f(E) [1 - f(E - \omega)]\} n(\omega). \end{aligned} \quad (8)$$

Quasiparticle-number conservation follows from the identities

$$\int_\Delta^\infty dE \rho(E) \text{St}_{\text{sp}}^{\text{phon}} = \int_\Delta^\infty dE \rho(E) \text{St}_{\text{st}}^{\text{phon}} = 0. \quad (9)$$

The recombination and pair-breaking terms are, respectively,

$$\text{St}_r^{\text{phon}}\{f, n\} = -\frac{1}{\tau_0 T_c^3} \int_{E+\Delta}^\infty d\omega \omega^2 U^+(E, \omega - E) f(E) f(\omega - E) [1 + n(\omega)] \quad (10)$$

and

$$\text{St}_{\text{PB}}^{\text{phon}}\{f, n\} = \frac{1}{\tau_0 T_c^3} \int_{E+\Delta}^\infty d\omega \omega^2 U^+(E, \omega - E) [1 - f(E)] [1 - f(\omega - E)] n(\omega). \quad (11)$$

Since the processes described by St^{phon} involve the emission or absorption of a phonon, in a general nonequilibrium situation one must also consider the kinetic equation for the phonon distribution function [9,19]:

$$\begin{aligned} \frac{dn(\omega)}{dt} &= \frac{2}{\pi \Delta_0 \tau_0^{\text{PB}}} \int_\Delta^\infty dE \rho(E) U^-(E, E + \omega) \{f(E + \omega) [1 - f(E)] [1 + n(\omega)] - f(E) [1 - f(E + \omega)] n(\omega)\} \\ &+ \frac{1}{\pi \Delta_0 \tau_0^{\text{PB}}} \int_\Delta^{\omega-\Delta} dE \rho(E) U^+(E, \omega - E) \{f(\omega - E) f(E) [1 + n(\omega)] - [1 - f(\omega - E)] [1 - f(E)] n(\omega)\} \\ &- \frac{1}{\tau_l} [n(\omega) - n_T(\omega, T_B)]. \end{aligned} \quad (12)$$

The first integral on the right-hand side is the counterpart to the quasiparticle-conserving collision integrals $\text{St}_{\text{sp}}^{\text{phon}}$ and $\text{St}_{\text{st}}^{\text{phon}}$ of Eqs. (5) and (8), while the second integral is the counterpart to the recombination and pair-breaking terms of Eqs. (10) and (11), the factor of 2 in front of the first integral accounting for spin. For frequencies $\omega < 2\Delta$, the second integral has to be replaced by zero. Within a phenomenological relaxation-time approach, the last term in Eq. (12) takes into account phonon exchange with a thermal-equilibrium bath of temperature T_B , $n_T(\omega, T_B) = (e^{\omega/T_B} - 1)^{-1}$. Note that the lifetime of a phonon of energy $2\Delta_0$ with regard to pair breaking at zero temperature τ_0^{PB} and the characteristic time τ_0 are related [12,22]:

$$\frac{\tau_0}{\tau_0^{\text{PB}}} = \frac{2\Delta_0 \pi \rho_F \omega_D^3}{9N_{\text{ion}} T_c^3}, \quad (13)$$

where ρ_F is the single-spin electronic density of states at the Fermi energy, ω_D is the Debye frequency, and N_{ion} is the ionic volume density. For Al, use of the parameters reported in Ref. [21] gives $\tau_0/\tau_0^{\text{PB}} \simeq 1.7 \times 10^3$, but this ratio is smaller for other materials considered there (for instance, it is about 36 for Nb).

B. Interaction with photons

For the photon collision integral, we consider a single mode of frequency $\omega_0 < 2\Delta$, so no photon-mediated recombination or pair breaking can occur. Then the collision integral resembles the number-conserving contribution to the phonon collision integral,

$$\begin{aligned} \text{St}^{\text{phot}}\{f, \bar{n}\} &= c_{\text{phot}}^{\text{QP}} U^+(E, E + \omega_0) \left\{ f(E + \omega_0) [1 - f(E)] (\bar{n} + 1) - f(E) [1 - f(E + \omega_0)] \bar{n} \right\} \\ &+ c_{\text{phot}}^{\text{QP}} U^+(E, E - \omega_0) \left\{ f(E - \omega_0) [1 - f(E)] \bar{n} - f(E) [1 - f(E - \omega_0)] (\bar{n} + 1) \right\}, \end{aligned} \quad (14)$$

and is itself number-conserving, $\int_{\Delta} dE \rho(E) \text{St}^{\text{phot}} = 0$. The term in the second curly brackets is set to zero for $E - \Delta < \omega_0$. Here the average photon number \bar{n} is treated as a known, independent quantity. More generally, it can be affected by the properties of the resonator, and in Sec. V we calculate \bar{n} as a function of the readout power for a half-wavelength resonator coupled to a transmission line. Following Ref. [11], we define an effective temperature T_0 via $e^{\omega_0/T_0} \equiv (\bar{n} + 1)/\bar{n}$. However, instead of approximating the density of states and coherence factors by their form near the gap, as done in Ref. [11], we keep their full form, and in contrast to Refs. [9,19] we include spontaneous photon emission. The coupling constant in resonators can be estimated as [23]

$$c_{\text{phot}}^{\text{QP}} = \frac{\delta}{2Q'}, \quad (15)$$

with Q' the quality factor of the resonator if the material resistivity were as in the normal state and $\delta \simeq 1/V\rho_F$ the mean level spacing, where V is the volume occupied by the quasiparticles. A schematic representation of the system considered is presented in Fig. 1.

C. Numerical approach

Equations (1)–(12) constitute a system of coupled nonlinear integral equations whose solution, even in the steady state, is clearly nontrivial. Here we describe briefly how we solve the system numerically. To discretize the system in the steady state, we divide the energy axis into

intervals $\Xi_i = [\psi_i, \psi_{i+1}]$, with $\psi_i = ih$, and average the kinetic equation over each such interval, so the steady-state condition for Eq. (1) becomes

$$\frac{d}{dt} \int_{\Delta+\psi_i}^{\Delta+\psi_{i+1}} dE f(E) = 0. \quad (16)$$

We choose the discretization such that the gap is an integer multiple of h , and additionally round the photon energy to the nearest integer multiple of h . Furthermore, for $E_i \in \Xi_i + \Delta$ and $\omega_j \in \Xi_j$, we approximate $f(E_i) = f(\Delta + \psi_i)$, $n(\omega_j) = n(\psi_j)$, and $K^{\pm}(E_i, E_i \pm \omega_j) = K^{\pm}(\Delta + \psi_i, \Delta + \psi_{i \pm j})$ to convert Eq. (1) to a system of ordinary equations. This procedure is equivalent to replacing the quasiparticle density of states by the density of states averaged over each interval Ξ_i and replacing the other quantities by their value on a grid as described above. A similar discretization procedure was used in Ref. [24]; the major differences from our work are that we discretize phonon and quasiparticle kinetic equations separately and ignore the variation of the coherence factors K^{\pm} and the factor ω^2 over each interval, enabling us to calculate the weights analytically [25]. We use the same approach of replacing the quasiparticle density of states by the averaged density of states, and discretizing the other quantities as described above, to obtain the discretized version of Eq. (12).

To arrive at the numerical solution of the full system, we proceed via intermediate steps that are similar to those we use to find approximate analytical results; see Secs. III

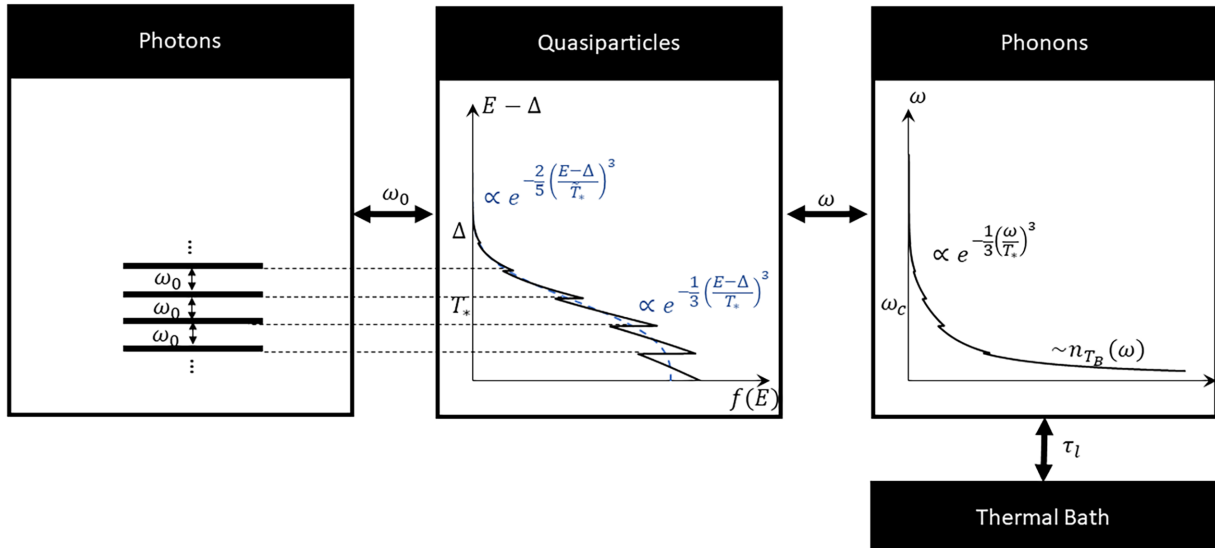


FIG. 1. The interaction of quasiparticles with photons and phonons. Absorption and emission of photons of frequency ω_0 drives the quasiparticle distribution out of equilibrium. The divergence in the BCS density of states leads to a quasiparticle distribution with peaks at multiples of the photon energy above the gap; the peaks' amplitudes follow a slowly varying (on the scale ω_0) envelope. The quasiparticles also exchange energy ω with the phonons in the superconductor; the phonons are in contact with a thermal bath, so their distribution can relax toward equilibrium over time τ_l .

and IV. To begin with, we take the phonon distribution to be the thermal-equilibrium phonon distribution, and keeping only terms linear in $f \ll 1$, we find Eq. (1) reduces to a matrix equation:

$$Mf^0 = 0, \quad (17)$$

where superscript 0 is used to denote the initial solution (i.e., step zero) for the quasiparticle distribution function. This equation can be solved by diagonalizing M but it does not determine the distribution's normalization. The latter is fixed by the nonlinear terms, and its approximate value can be found with use of the discretized version of the approach described in Sec. IV.

After obtaining the properly normalized f^0 , we can take into account nonlinear terms in Eqs. (1) and (12) using Newton's algorithm. To solve the two equations simultaneously, we follow Ref. [12] by forming the state vector $x = (f, n)^T$ and writing the system of equations determining the state vector in the steady state in the form $g(x) = 0$. Successive approximations x^i to the state vector are calculated with use of the recursive relation

$$x^{i+1} = x^i - J^{-1}(x^i)g(x^i), \quad (18)$$

with J^{-1} the inverse of the Jacobian matrix of g . The normalized f^0 is used as the initial guess for the quasiparticle distribution, while the initial guess for the phonon distribution can be obtained by inserting f^0 in Eq. (12), setting the temporal derivative to zero, and solving that linear equation for n . Calculations of the initial phonon distribution and of the Jacobian matrix can be done analytically, thus avoiding long computational times and rounding errors.

The discretized system of equations is not differentiable with respect to the gap Δ , so we do not include the self-consistency condition, Eq. (2), in Newton's algorithm. To find deviations of the gap from its equilibrium value, we can solve Eq. (18) for a fixed gap. This gives the distribution f as a function of the gap, and we can use the result in a bisection algorithm applied to Eq. (2) to calculate the nonequilibrium gap. While this method gives a fully self-consistently calculated gap, it is accurate only up to variations of the gap of order h , as both the gap and the photon energy have to be rounded to an integer multiple of h in the calculation of the distribution function. For the small deviation $\delta = \Delta_0 - \Delta$ of the gap from its zero-temperature value encountered in this work, we instead proceed as follows: the left-hand side of Eq. (2) is approximately δ/Δ_0 at leading order; therefore, in an iterative approach to solving the equation, we calculate f with the gap fixed at its thermal-equilibrium value, thus ignoring the deviation of the gap from equilibrium on the right-hand side. This gives an expression for δ in terms of an integral that depends only on the quasiparticle distribution obtained with use of the thermal-equilibrium gap

and that can be evaluated numerically. The numerical solution gives the quasiparticle distribution at points on an energy grid of spacing h ; since we want to use a finer grid to numerically evaluate the integral, between these points we linearly interpolate the distribution function (the interpolation can be used because the distribution function is smooth between two nearby peaks at multiples of ω_0 above the gap).

D. Relevant timescales

While a numerical solution to the system of coupled integral equations, Eqs. (1) and (12), can be found as just described, an exact analytical solution is likely impossible except in particular cases such as thermal equilibrium; it is therefore instructive to discuss the different timescales governing the dynamics of the quasiparticles and phonons and under which conditions approximate analytical solutions might be found. Throughout this work we assume the quasiparticles to be nondegenerate, $f(E) \ll 1$, so we always ignore Pauli-blocking factors by using the replacement $[1 - f(E)] \rightarrow 1$.

There are several characteristic times that can be read off from the kinetic equations, as detailed in Appendix A. These lifetimes, in general, depend on the energy E of the quasiparticle or ω of the phonon; we begin by discussing the phonon lifetimes. For phonons with energy above the pair-breaking threshold, $\omega > 2\Delta$, their pair-breaking lifetime $\tau_{\text{PB}}^{\text{phon}}(\omega)$ depends weakly on energy near the threshold, so we take $\tau_{\text{PB}}^{\text{phon}}(\omega) \approx \tau_0^{\text{PB}}$; in Al, $\tau_0^{\text{PB}} \simeq 240$ ps [21]. The lifetime due to the phonon being absorbed by a quasiparticle is, in general, much longer than this, $\tau_{\text{abs}}^{\text{phon}}(\omega) \gg \tau_0^{\text{PB}}$, due to the assumed nondegeneracy (and hence low density) of the quasiparticles. In contrast, in aluminum films the thermalization time τ_l [last term in Eq. (12)] is comparable to the pair-breaking time, $\tau_l \sim \tau_0^{\text{PB}}$; for films of thickness 100 nm on a sapphire substrate, the thermalization time is estimated to be approximately 500 ps [19,26,27]. Since thermalization and pair-breaking times are comparable, we expect them both to have an impact on the above-threshold phonon distribution and hence on the quasiparticle number. Moreover, the absorption time being long means that the phonon distribution can significantly deviate from the equilibrium phonon distribution; however, as we discuss below, generally this does not impact the shape of the quasiparticle distribution. We note that these considerations can be material specific; for instance, for a 100-nm-thick Nb film on sapphire we estimate $\tau_0^{\text{PB}} \simeq 4$ ps and $\tau_l \simeq 1.5$ ns [21,26], so deviations from equilibrium can become more significant compared with the aluminum case.

Turning to the quasiparticle lifetimes, we can identify two scattering times, $\tau_{s,t}^{\text{QP}}(E)$ and $\tau_{s,n}^{\text{QP}}(E)$, involving phonons and phonons, respectively, and accounting for all possible number-conserving processes (absorption as well

as spontaneous and stimulated emission), and the recombination lifetime $\tau_r^{\text{QP}}(E)$, which is inversely proportional to the quasiparticle density. In this work we focus on quasiparticles of energies up to a few times the superconducting gap, as the energy dependence of the phonon scattering time implies that quasiparticles of higher energies typically relax very quickly toward the gap and therefore do not contribute directly to processes such as photon absorption. When the recombination lifetime is longer than the scattering lifetimes, $\tau_r^{\text{QP}} \gg \tau_{s,n}^{\text{QP}}, \tau_{s,t}^{\text{QP}}$, as is the case for low quasiparticle densities and sufficiently high photon number, the shape of the quasiparticle distribution function is determined by the number-conserving processes, while generation and recombination affect its normalization (i.e., the overall quasiparticle density). Moreover, for strong deviations from equilibrium to be possible, the photon scattering time should be the shortest timescale, $\tau_{s,t}^{\text{QP}} \lesssim \tau_{s,n}^{\text{QP}}$, a condition that can be met if the number of photons \bar{n} is sufficiently large and/or the phonon bath temperature T_B sufficiently low; in particular, the phonon scattering time being longer than the photon scattering time means that deviations of the phonon distribution from equilibrium have a small effect on the shape of the quasiparticle distribution (see also Sec. III C). Therefore, in the next section we study the shape of the quasiparticle distribution function starting with the case of zero phonon temperature and then generalizing to finite temperature. Interestingly, we show that despite the assumption of low T_B , stimulated emission and absorption of phonons cannot be ignored at all energies and that they determine the high-energy tail of the distribution function.

III. SHAPE OF THE QUASIPARTICLE DISTRIBUTION FUNCTION

As discussed in Sec. I, our goal is to find the quasiparticle distribution function by approximately solving the system of coupled equations (1), (2), and (12) in the steady state in the regime of low temperatures, and hence low quasiparticle density, and high number of photons, $\bar{n} \gg 1$, or equivalently $T_0 \gg \omega_0$. A sufficient condition for having low density is $f(E) \ll 1$, which enables us to approximate the Pauli-blocking factors as $[1 - f(E)] \approx 1$. Moreover, we ignore in this section the recombination and pair-breaking collision integrals, Eqs. (10) and (11), since they affect the normalization but not the shape of the quasiparticle distribution function, as argued in Sec. II D.

At low temperature $T_B \ll \omega_0$, the competition between absorption of photons and emission of phonons results in a quasiparticle distribution with peaks at energies $\Delta + m\omega_0$, $m = 0, 1, 2, \dots$ [11,12]. Here we focus on the envelope function that determines the heights of these peaks. Then interpreting $f(E)$ as this envelope, we can approximately write the photon collision integral, Eq. (14), as a

generalized diffusion operator in energy space,

$$\text{St}^{\text{phot}}\{f, \bar{n}\} \simeq c_{\text{phot}}^{\text{QP}} \frac{\omega_0^2}{U^+(E, E)} \bar{n} \frac{\partial}{\partial E'} \left[U^+(E, E')^2 e^{-E'/T_0} \times \frac{\partial}{\partial E'} \left(f(E') e^{E'/T_0} \right) \right] \Big|_{E'=E}, \quad (19)$$

as one can verify by Taylor expansion of Eq. (14) to second order in ω_0 . Next we consider explicitly three cases (1) phonons in equilibrium at zero temperature; (2) phonons in equilibrium at finite temperature; (3) nonequilibrium corrections to the phonon distribution function.

A. Phonons in equilibrium at $T_B = 0$

The assumption that phonons are in equilibrium corresponds to taking the limit $\tau_l \rightarrow 0$ in Eq. (12), so $n(\omega) = n_T(\omega, T_B)$ is the (leading-order) solution for the phonon distribution function. For $T_B = 0$, this implies $n(\omega) = 0$, and the steady-state equation for the quasiparticle distribution function reduces to

$$0 = \text{St}_{\text{sp}}^{\text{phon}}\{f\} + \text{St}^{\text{phot}}\{f, \bar{n}\}, \quad (20)$$

with $\text{St}_{\text{sp}}^{\text{phon}}$ of Eq. (5) and St^{phot} of Eq. (19). Even this much-simplified equation cannot be solved exactly, so we consider separately three energy ranges—low, intermediate, and high—to be defined below. In all three ranges we assume the photon number to be so large that T_0 is the highest energy scale; then we can take the limit $T_0 \rightarrow \infty$ in Eq. (19) and replace the exponential factors with unity.

The low-energy and intermediate-energy ranges are sufficiently close to the gap, $E - \Delta \ll \Delta$, so one can approximate

$$U^+(E_1, E_2) \simeq \sqrt{\frac{2\Delta}{E_2 - \Delta}} \quad (21)$$

for $E_2 > \Delta$ and $U^+ = 0$ otherwise in Eq. (19) and

$$U^-(E_1, E_2) \simeq \frac{E_1 + E_2 - 2\Delta}{\sqrt{2\Delta(E_2 - \Delta)}} \quad (22)$$

in Eq. (5). Within this approximation, $\text{St}_{\text{sp}}^{\text{phon}}\{f\}$ takes the form

$$\begin{aligned} \text{St}_{\text{sp}}^{\text{phon}}\{f\} = & -\frac{128}{105\sqrt{2}} \left(\frac{\Delta}{T_c}\right)^3 \left(\frac{E - \Delta}{\Delta}\right)^{7/2} \frac{f(E)}{\tau_0} \\ & + \frac{1}{\tau_0 T_c^3} \int_0^\infty d\omega \omega^2 \frac{2E - 2\Delta + \omega}{\sqrt{2\Delta(E + \omega - \Delta)}} \\ & \times f(E + \omega). \end{aligned} \quad (23)$$

Introducing the temperature scale

$$T_* \equiv \left(\frac{105}{64} T_c^3 c_{\text{phot}}^{\text{QP}} \bar{n} \tau_0 \omega_0^2 \Delta \right)^{1/6} \quad (24)$$

characterizing the width of the distribution function and ignoring the first term on the right-hand side in Eq. (23) for $E - \Delta \lesssim T_*$ (low energy range) and the second one for $T_* \lesssim E - \Delta \lesssim \Delta$ (intermediate range) leads to the solution derived in Ref. [11]:

$$f(x) \simeq \begin{cases} b_0 (1 - 0.564x^{5/2} + 0.119x^{7/2}), & x \lesssim 1, \\ 3b_0 \text{Ai} \left(\frac{x^2}{4^{1/3}} \right), & 1 \lesssim x \ll \Delta/T_*, \end{cases} \quad (25a)$$

$$(25b)$$

with $x \equiv (E - \Delta)/T_*$, Ai the Airy function, and b_0 a normalization constant whose determination is the subject of Sec. IV. Note that depending on the parameters (and in particular by increasing \bar{n}) the intermediate regime could be absent; here we assume for simplicity that the condition $T_* < \Delta$ is satisfied (this is consistent with considering quasiparticles with energies up to a few times the gap; see Sec. IID). Moreover, the initial assumptions that T_0 is large and that we can study the envelope concretely means $T_0 \gg T_* \gg \omega_0$.

In the high-energy range $E - \Delta \gtrsim \Delta$, we ignore terms of order $(\Delta/E)^2$ in Eq. (19), leading to

$$\text{St}^{\text{phot}}\{f, \bar{n}\} = \bar{n} c_{\text{phot}}^{\text{QP}} \omega_0^2 f''(E). \quad (26)$$

Since for $T_* < \Delta$ most quasiparticles are at energies below 2Δ , at energies $E > 2\Delta$ the first integral in Eq. (5) is much smaller than the second one and can be ignored; therefore, we can further approximate

$$\text{St}_{\text{sp}}^{\text{phon}} \simeq -\frac{f(E)(E-\Delta)^3}{\tau_0 T_c^3} \quad (27)$$

in the high-energy regime. Using the substitution $\tilde{x} \equiv (E - \Delta)/T_*$, with

$$\tilde{T}_* \equiv (3\bar{n} c_{\text{phot}}^{\text{QP}} \omega_0^2 \tau_0 T_c^3)^{1/5} = \left(\frac{64}{35} \frac{T_*}{\Delta} \right)^{1/5} T_*, \quad (28)$$

in Eq. (20), that equation takes the form of a generalized Airy equation,

$$f''(\tilde{x}) - \tilde{x}^3 f(\tilde{x}) = 0. \quad (29)$$

The solution to this equation can be written in terms of a

modified Bessel function of the second kind:

$$f(\tilde{x}) = \tilde{b}_0 \sqrt{\tilde{x}} K_{1/5} \left(\frac{2}{5} \tilde{x}^{5/2} \right). \quad (30)$$

With our assumptions we are interested only in the limit of large \tilde{x} , so we can approximate

$$f(\tilde{x}) \simeq \tilde{b}_0 \sqrt{\frac{5\pi}{4\tilde{x}^{3/2}}} e^{-2\tilde{x}^{5/2}/5}. \quad (31)$$

This expression should match the similar approximation for Eq. (25b) at an energy of order 2Δ . Indeed, the exponential factors are identical at $E = 143\Delta/80$, and the prefactors are then related by

$$\frac{\tilde{b}_0}{b_0} = \frac{3^{3/2} 2^{2/3}}{5\pi} \left(\frac{64}{35} \frac{T_*}{\Delta} \right)^{-2/5}. \quad (32)$$

Because of the faster-than-exponential decay of the distribution over the energy scale $T_* \lesssim \Delta$, it might seem irrelevant to calculate here and in the next subsection the behavior of its high-energy tail ($E \gtrsim 2\Delta$); however, quasiparticles with energy above 3Δ can relax by emitting a pair-breaking phonon, which in turn can generate two quasiparticles. That is why knowledge of the tail is needed to understand how the photons influence the quasiparticle density; see Sec. IV.

B. Equilibrium phonons, $T_B > 0$

We now consider in more detail the effect of thermal phonons. We aim to show that ignoring phonons is a good approximation up to a crossover energy E_* , above which the (envelope of the) quasiparticle distribution function takes the thermal-equilibrium form. Using Eq. (8), we define the energy scale E_* as that energy at which the equation

$$\text{St}_{\text{st}}^{\text{phon}}\{f, n_T\} + \text{St}^{\text{phot}}\{f, \bar{n}\} = 0 \quad (33)$$

is satisfied, with f as obtained in Sec. III A and $n = n_T$ being the thermal distribution of phonons.

By the definition of E_* , up to that energy we can ignore the phonons and hence Eq. (20) holds; that equation enables us to express St^{phot} in terms of $\text{St}_{\text{sp}}^{\text{phon}}$. For the latter, at high energies $E - \Delta \gg \Delta$, we can use Eq.(27) to get

$$\text{St}^{\text{phot}}\{f, \bar{n}\} = -\text{St}_{\text{sp}}^{\text{phon}}\{f\} \simeq \frac{(E - \Delta)^3}{3\tau_0 T_c^3} f(E), \quad (34)$$

with $f(E)$ decreasing faster than exponentially; see Eq. (31). To estimate E_* using Eq. (33) we need an approximate expression for $\text{St}_{\text{st}}^{\text{phon}}$. It turns out that the main contribution to this collision integral originates from the

term in Eq. (8) proportional to $f(E - \omega)$, since as a function of ω that factor increases faster than exponentially (as long as $E - \omega$ remains sufficiently large); thus, it dominates over the exponential suppression of $n(\omega, T_B)$ at $\omega \gg T_B$, leading to a sharply peaked maximum of the integrand at a certain energy ω_M , as detailed in Appendix B. Introducing the crossover temperature

$$T_B^* \equiv \left(\frac{T_*}{\Delta}\right)^3 \Delta = \omega_0 \sqrt{\frac{105}{64} c_{\text{phot}}^{\text{QP}} \bar{n} \tau_0} \left(\frac{T_c}{\Delta}\right)^{3/2}, \quad (35)$$

we can distinguish two regimes: for low phonon temperature and high photon number, $T_B \ll T_B^*$, we find

$$E_* \approx \Delta + \tilde{T}_* (\tilde{T}_*/T_B)^{2/3} \gtrsim 2\Delta, \quad (36)$$

while for high phonon temperature and low photon number, $T_B^* \lesssim T_B \ll T_*$, we get

$$E_* \approx \Delta + T_* (T_*/T_B)^{1/2} \lesssim 2\Delta. \quad (37)$$

In both cases, it turns out that for $E > E_*$, stimulated emission and absorption of phonons dominates over the interaction with photons, so the distribution function is approximately of the Boltzmann form,

$$f(E) \simeq b_T e^{-E/T_B}, \quad (38)$$

where b_T can be found by requiring continuity of f at $E = E_*$. Note that while here the ratio between T_B and T_B^* being below or above unity has the apparently minor role of determining whether E_* is above or below 2Δ , we later see that this ratio influences also the temperature dependence of both the quasiparticle density and the quality factor.

C. Finite thermalization time

So far we have assumed that the phonon distribution has the equilibrium form, corresponding to the limit of zero thermalization time τ_l . If the thermalization time is nonzero, the phonon distribution can deviate from the equilibrium phonon distribution, as discussed in Sec. IID. We can distinguish between phonons of energy ω below and above the pair-breaking threshold 2Δ . Above-threshold phonons can break Cooper pairs and thus influence the quasiparticle density—this is the subject of Sec. IV. These phonons can also affect the shape of the quasiparticle distribution by being absorbed, but these processes are far-less frequent than pair breaking (since $\tau_{\text{abs}}^{\text{phon}} \gg \tau_0^{\text{PB}}$) and the change would occur only at high energies $E > 3\Delta$ where the occupation is generically extremely small, so we ignore this effect.

Below-threshold phonons, in contrast, can affect the quasiparticle distribution at all energies. However, we

now show that significant deviations from the equilibrium phonon distribution appear only at relatively high energy ω and have a negligible effect on the shape of the quasiparticle distribution. Indeed, for $\omega < 2\Delta$ we can approximately solve Eq. (12) in the steady state, writing $n(\omega) \simeq n_T(\omega, T_B) + n_1(\omega)$, with (see Appendix C for details)

$$n_1(\omega) \simeq \frac{2\tau_l}{\pi \Delta_0 \tau_0^{\text{PB}}} \int_{\Delta}^{\infty} dE \rho(E) U^-(E, E + \omega) f(E + \omega), \quad (39)$$

and the n_1 term becomes dominant above the crossover energy

$$\omega_c \approx T_B \ln \left(\frac{\Delta}{T_*} \frac{\tau_0^{\text{PB}}}{\tau_l} b_0^{-1} \right) \quad (40)$$

(this approximate expression is valid for $T_* \lesssim \omega_c \ll T_* \sqrt{3T_*/T_B}$ and $\omega_c \lesssim \Delta$; see Appendix C for a more-accurate determination of ω_c). The crossover energy depends on the quasiparticle density through $b_0 \ll 1$, which cannot be determined without considering the nonlinear terms in the kinetic equations. However, for thermalization time τ_l short compared with τ_0^{PB} , we expect the density to be comparable to the density in thermal equilibrium, and hence $b_0 \sim e^{-\Delta/T_B}$ (the quasiparticle density is discussed in more detail in Sec. IV); this implies that ω_c would become larger than Δ and grow with decreasing τ_l or T_* , as one would expect, since reducing these parameters means that the system is closer to thermal equilibrium. We return to this point when comparing our results with numerical calculations in Sec. IV C.

To determine if n_1 influences the shape of the distribution function f , one can proceed as in Sec. III B, by the replacement $n_T \rightarrow n_T + n_1$ in Eq. (33). As mentioned there, the main contribution of n_T to the collision integral $\text{St}_{\text{st}}^{\text{phon}}$ comes from the region around an energy ω_M ; if this energy is smaller than ω_c , we expect negligible impact of n_1 on the shape of f . This is clearly the case in the limit of fast phonon thermalization $\tau_l \rightarrow 0$, since in this case, as discussed above, $\omega_c > \Delta$, while, in general, $\omega_M < \Delta$ (see Appendix B), so $\omega_M < \omega_c$. We do not investigate here more generally when the condition $\omega_M < \omega_c$ is satisfied, or the effect of n_1 on f when it is violated, but we show numerically that for experimentally relevant parameters the shape of f derived in this section is valid at least up to energies of a few times Δ .

IV. QUASIPARTICLE DENSITY

The considerations in the previous section are limited to the shape of the quasiparticle distribution function, including the effect of nonequilibrium phonons due to finite thermalization time; see Sec. III C. However, it follows

from the pair-breaking phonon collision integral, Eq. (11), that nonequilibrium phonons can potentially affect the quasiparticle number as soon as the crossover frequency ω_c between the equilibrium phonon population and the nonequilibrium phonon population satisfies $\omega_c \lesssim 2\Delta$, a weaker condition than that required for them to affect the shape of the distribution function, $\omega_c < \omega_M$. Consequently, in this section we investigate the effect a nonzero thermalization time has on the number of quasiparticles in the regime $\omega_M < \omega_c \lesssim 2\Delta$, in which the influence of nonequilibrium phonons on the shape of the quasiparticle distribution can be ignored, while their influence on the quasiparticle density must be established.

The quasiparticle density N_{QP} is given by

$$N_{\text{QP}} \equiv 4\rho_F \int_{\Delta}^{\infty} dE \rho(E) f(E) \simeq 4.2\rho_F \sqrt{2\Delta T_*} b_0, \quad (41)$$

where for f we use the distribution function from Sec. III and the numerical prefactor was determined in Ref. [11]. As remarked previously, to find the value of the normalization constant b_0 , the recombination and pair-breaking collision integrals, Eqs. (10) and (11), must be taken into account. To do so, we multiply the kinetic equation, Eq. (1), by the BCS density of states $\rho(E)$, integrate the resulting equation over energy E , and assume the steady-state condition $df/dt = 0$ to arrive at the equation

$$\int_{\Delta} dE \rho(E) \int_{E+\Delta} d\omega \omega^2 U^+(E, \omega - E) \times [n(\omega) - f(E)f(\omega - E)] = 0, \quad (42)$$

where, as before, we ignore Pauli-blocking factors and assume $n(\omega) \ll 1$ for $\omega > 2\Delta$. The two terms in square brackets originate from pair breaking and recombination, respectively. For the former, we can switch the integration order and realize that the resulting integral over E is the same as that determining the lifetime of phonons with regard to pair breaking (see Appendix A); ignoring again the weak dependence of the result on ω , we rewrite the above equation as

$$\int_{2\Delta} d\omega \omega^2 \left[n(\omega) - \frac{1}{\pi\Delta} \int_{\Delta}^{\omega-\Delta} dE \rho(E) \times U^+(E, \omega - E) f(E) f(\omega - E) \right] = 0. \quad (43)$$

To proceed further, we need to know the phonon distribution function above the pair-breaking threshold, $\omega > 2\Delta$; as shown in Appendix C, it takes the form

$$n(\omega) \simeq \frac{\tau_0^{\text{PB}}}{\tau_l + \tau_0^{\text{PB}}} [n_T(\omega, T_B) + n_1(\omega) + n_2(\omega)], \quad (44)$$

with n_1 of Eq. (39) and n_2 being equal to the product of $\tau_l/\tau_0^{\text{PB}}$ and the second term in square brackets in Eq. (43).

Equation (43) can now be recast as a quadratic equation for b_0 (see Appendix D):

$$I_2 b_0^2 - 2 \frac{\tau_l}{\tau_0^{\text{PB}}} I_1 b_0 - I_0 = 0, \quad (45)$$

with the quadratic term arising from the pair-breaking contribution together with n_2 , the linear term from n_1 , and the constant term from n_T . Because of their origins, I_0 and I_2 are dimensionless functions of T_B/Δ and T_*/Δ , respectively, while I_1 depends, in general, on both. We can distinguish two limiting cases: If $(\tau_l I_1 / \tau_0^{\text{PB}})^2 \ll I_2 I_0$, then (see Appendix D)

$$b_0 \simeq \sqrt{I_0/I_2} \simeq \sqrt{\pi T_B/T_*} e^{-\Delta/T_B} / 2.1, \quad (46)$$

and the quasiparticle density is approximately the same as in thermal equilibrium, even though the distribution function differs significantly from the equilibrium one. In the opposite limit we find that $b_0 \simeq 2\tau_l I_1 / \tau_0^{\text{PB}} I_2$ is larger than the thermal-equilibrium value and is proportional to the ratio $\tau_l/\tau_0^{\text{PB}}$: the larger this ratio (i.e., the greater τ_l), the easier it is to enter into this limit and the larger the quasiparticle density. We discuss further the corresponding nonequilibrium quasiparticle density in the framework of a generalized Rothwarf-Taylor (RT) model.

A. Generalized RT model

Given the proportionality between b_0 and N_{QP} , Eq. (41), the last and first terms on the left-hand side of Eq. (45) correspond exactly to the phonon-generation and quasiparticle-recombination terms in the steady-state version of the Rothwarf-Taylor model [28] (we do not consider here direct quasiparticle injection). We can relax the steady-state assumption and allow for variation in time of parameters such as bath temperature (T_B) and photon number (i.e., T_*), as long as their change is slow on the scale over which the shape of the distribution function is established, namely, the quasiparticle scattering times; see Sec. II D (note that since τ_0^{PB} is less than τ_0 , the phonon distribution quickly follows any change in the quasiparticle distribution). Then the shape of the distribution function is at all times the one we calculate in Sec. III, and integration over energy of the kinetic equation times $4\rho_F \rho(E)$ gives

$$\frac{dN_{\text{QP}}}{dt} = G_T + G(T_*/\Delta) N_{\text{QP}} - R N_{\text{QP}}^2, \quad (47)$$

where

$$G_T = \frac{16\pi\rho_F\Delta}{\bar{\tau}_0} \left(\frac{\Delta}{T_c} \right)^3 \frac{T_B}{\Delta} e^{-2\Delta/T_B} \quad (48)$$

is the rate of quasiparticle generation (per unit volume) due to thermal phonons for T_B small compared with 2Δ , and

$$R = \frac{2\Delta^2}{\rho_F \bar{\tau}_0 T_c^3} \quad (49)$$

is the quasiparticle-recombination coefficient. Both quantities are renormalized by the finite phonon thermalization time, an effect known as ‘‘phonon trapping’’[19],

$$\bar{\tau}_0 = \tau_0(1 + \tau_l/\tau_0^{\text{PB}}). \quad (50)$$

Note that as T_* approaches Δ , corrections to R and τ_0^{PB} resulting from the finite distribution’s width, of order T_*/Δ , can become relevant, as discussed in Appendix E.

The central term on the right-hand side of Eq. (47) is absent in the Rothwarf-Taylor model, and represents an additional quasiparticle-generation term proportional to the quasiparticle density itself. It originates from pair-breaking nonequilibrium phonons emitted by quasiparticles that have been excited to sufficiently high energies by the photons. Indeed, the coefficient can be taken in the form (see the end of Appendix D)

$$G(x) = \frac{\gamma}{\bar{\tau}_0 \tau_0^{\text{PB}}} \left(\frac{\Delta}{T_c}\right)^3 x^{9/2} e^{-\sqrt{14/5}x^{-3}}, \quad (51)$$

with $\gamma = 2^{13/6}3^{3/2}/(2.1 \times 5\sqrt{7}) \simeq 0.84$, and vanishes if the phonons are forced to be in thermal equilibrium ($\tau_l = 0$). At high phonon temperature and low photon number, $T_B \gtrsim T_B^*$, this term can be ignored, and in the steady state the quasiparticle density approximately takes the thermal-equilibrium value; in the opposite regime, $T_B \ll T_B^*$, it leads to a quasiparticle density independent of the bath temperature T_B and larger than that in thermal equilibrium. Although the linearity in N_{QP} of this additional generation term could be expected—the more quasiparticles there are, the more can be excited to high energy and emit phonons—we stress that the dependence on the photon number can be found only after solving the kinetic equation for the shape of the distribution function; therefore, it is beyond the reach of phenomenological treatments that consider just the quasiparticle density from the outset. In this regime the quasiparticle density is strongly dependent on the photon number; the strong dependence originates from the fact that only quasiparticles in the high-energy tail of the distribution function, $E > 3\Delta$, can emit pair-breaking photons, and a quasiparticle must absorb a large number of photons to reach that energy while also losing energy by emitting phonons. Note that in the extreme case $T_B = 0$, the solution $N_{\text{QP}} = 0$ is unstable: even a single quasiparticle can start the process of driving the phonons out of equilibrium and hence generate more quasiparticles. In Fig. 2 we provide an overview of the different regimes we identify and of the parameter regions where our approach is applicable.

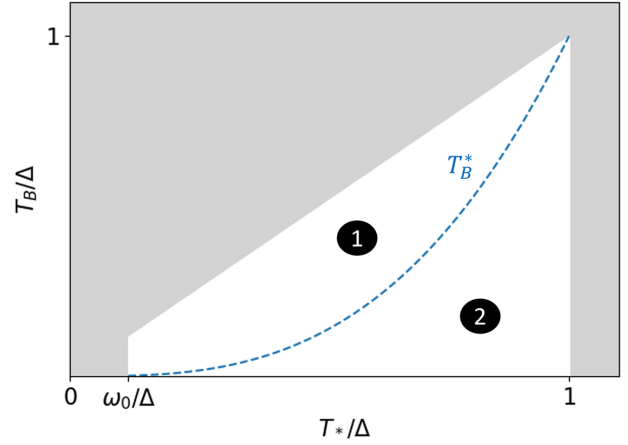


FIG. 2. Depending on the phonon temperature T_B and the photon number \bar{n} [i.e., T_* in Eq. (24)], there are two regimes for the quasiparticle density. In regime 1, thermal phonons dominate quasiparticle creation and the quasiparticle density is approximately as in equilibrium. In regime 2, the photons drive a sufficient amount of quasiparticles to energies $E > 3\Delta$ such that quasiparticle creation from phonons emitted by these high-energy quasiparticles is dominant; in this regime, the quasiparticle density is larger than in equilibrium and depends on the photon number but not on the temperature of the phonon bath. The crossover between the two regimes occurs when $T_B \sim T_B^*/\Delta^2$ [see Eq. (35)], as indicated by the dashed curve. The area shaded in gray ($T_* < \omega_0$, $T_* > \Delta$, $T_B > T_B^*$) identifies the parameter regions where approximations made in the analytical derivations are not valid.

B. Gap suppression

Once the normalization constant b_0 is found using Eq. (45) [or, equivalently, N_{QP} is found using Eq. (47)], we can perturbatively calculate the change in the gap $\delta\Delta = \Delta_0 - \Delta$. Indeed, substituting the distribution function of Sec. III into Eq. (2), we find

$$\frac{\delta\Delta}{\Delta_0} = 4.2b_0 \sqrt{\frac{T_*}{2\Delta_0}} \left(1 - \frac{1}{4} \frac{0.88 T_*}{2.1 \Delta_0}\right), \quad (52)$$

where we use the numerical estimate $\int_0^1 dx \sqrt{xf}(x) \simeq 0.88$ [in the perturbative calculation we ignore the deviation of Δ from Δ_0 on the right-hand side of Eq. (2); this is consistent if $T_*/\Delta_0 \gg b_0^2$]. The leading-order term is equal to the leading-order approximation for $N_{\text{QP}}/(2\rho_F \Delta_0)$ [see Eq. (41)], which is the fraction of broken Cooper pairs; this result is generic to quasiparticles whose distribution-function width above the gap (in our case, T_*) is small compared with the gap itself. Including corrections up to second order in T_*/Δ , we can rewrite Eq. (52) in the form

$$\frac{\delta\Delta}{\Delta_0} = \frac{N_{\text{QP}}}{2\rho_F \Delta_0} \left[1 - 0.42 \frac{T_*}{\Delta_0} + 0.22 \left(\frac{T_*}{\Delta}\right)^2\right]. \quad (53)$$

For comparison, in thermal equilibrium the terms in square brackets read $1 - 0.5T_B/\Delta_0 + 3(T_B/\Delta_0)^2/8$; this shows that for a given quasiparticle density, the gap is less suppressed in the nonequilibrium case, since by assumption $T_* > T_B$. We can therefore find an enhancement of superconductivity, since for $T_B \gtrsim T_B^*$ the quasiparticle density takes roughly the same value as in equilibrium (more accurately, the quasiparticle density slightly decreases with increasing T_* in this regime, as discussed in Appendix E, and thus the enhancement is even stronger). In the opposite case, the density is much larger than in equilibrium and hence superconductivity is weakened.

C. Comparison with numerical calculations

As a validation of our approach, we now compare the analytical results with the numerical solution of the full system of kinetic equations, Eqs. (1)–(12). Unless otherwise stated, in this subsection we use the parameters listed in Table I. Their values are chosen to enable the comparison with experiments that is discussed in the next section; that is, they should be typical for thin-aluminum-film resonators. The critical temperature is assumed to be connected to the gap via the BCS relation $\Delta_0 = 1.764T_c$, resulting in $T_c \simeq 1.18$ K. Using Eq. (13) and the assumed τ_0 , we find the phonon lifetime with regard to pair breaking τ_0^{PB} is 255 ps. The parameters loosely satisfy the validity conditions for the analytical approximations, namely, $\omega_0 \ll T_* \lesssim \Delta$, $b_0 \ll 1$, and $\omega_c > \omega_M$ (b_0 can be read off Fig. 3; using the results in Appendix B, we calculate $\omega_M \simeq 0.57\Delta_0$, while ω_c can be estimated from Fig. 4). For the numerical calculations, we take $h = \Delta_0/180$ for the discretization step size and truncate the energy at $E_{\text{max}} = 10\Delta_0$; note that $\omega_0 = 20h$, meaning the shape of the peaks is captured by the numerical calculations.

In Fig. 3 we plot with solid lines the numerically calculated quasiparticle distribution function f as function of energy for different values of the thermalization time τ_l . In all cases, we find good agreement with the analytical predictions (dashed lines) of Sec. III spanning several orders of magnitude in occupation probability, whose large variation occurs over an energy range of a few times the gap. For $\tau_l = 0$, the phonons are at thermal equilibrium and the high-energy tail of f approaches the expected exponential decay; see Sec. III B. As τ_l increases, however, the high-energy tail deviates significantly from the $\tau_l = 0$ prediction; the reason for this deviation is the reabsorption

TABLE I. Parameters used for the plots in Figs. 3 and 4. The quantities T_* and T_B^* are calculated from the other parameters with use of their respective definitions, Eqs. (24) and (35).

$c_{\text{phot}}^{\text{QP}}$	τ_0	Δ_0	ω_0	\bar{n}	T_B	T_*	T_B^*
1 Hz	438 ns	180 μeV	$\Delta_0/9$	10^7	0.1 K	$\Delta_0/2$	0.26 K

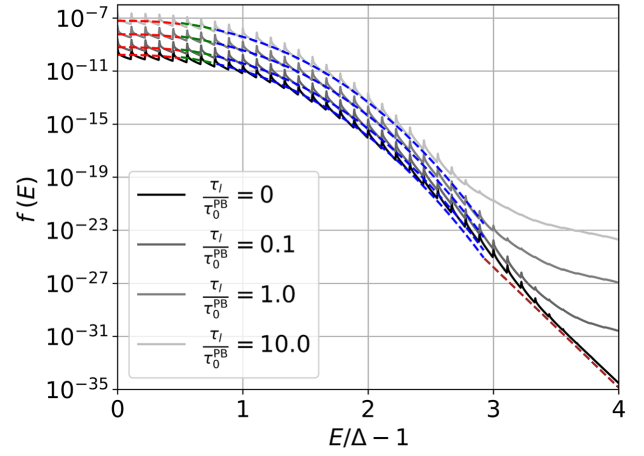


FIG. 3. Quasiparticle distribution function versus energy for the parameters in Table I. Solid gray lines shows the results of numerical calculations. The dashed colored lines are obtained with use of the analytical approximations in their respective regimes of applicability; from left to right: Eqs. (25a), (25b), (31), and (for $\tau_l = 0$) Eq. (38). The normalization coefficient b_0 is calculated by use of the steady-state solution to Eq. (47) in Eq. (41) (we take into account the corrections to the recombination coefficient and the quasiparticle density discussed in Appendix E).

of phonons emitted by recombination processes [see n_2 in Eq. (44)], which have energy $\omega > 2\Delta$. Consequently, the deviation occurs at energies above 3Δ . At those energies for $T_* \lesssim \Delta$ the occupation probability is so small that the deviation does not affect the quasiparticle density.

Figure 4 shows the phonon distribution function versus energy ω . There are no visible deviations from the thermal-equilibrium behavior up to the τ_l -dependent energy ω_c (see Sec. III C) for all values of τ_l considered. For ω between ω_c

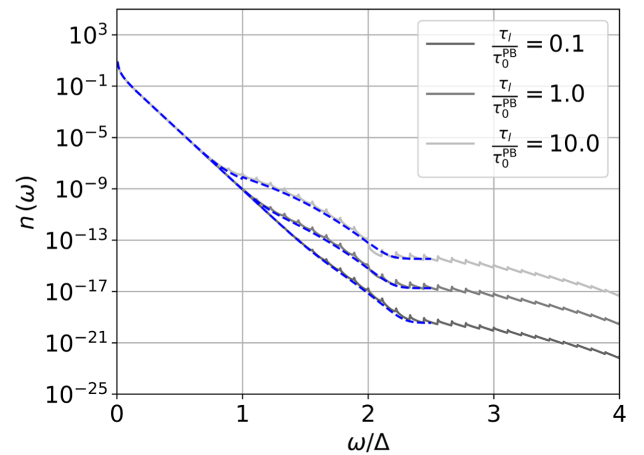


FIG. 4. Phonon distribution for the system simulated in Fig. 3. The dashed blue lines in the phonon distribution are the analytical results derived in Appendix C, and the solid gray lines are simulation results.

and 2Δ , phonons spontaneously emitted by the nonequilibrium quasiparticles become relevant and the phonon distribution function is predominantly given by $n_1(\omega)$ of Eq. (39) (see also Appendix C). For $\omega > 2\Delta$ the recombination of nonequilibrium quasiparticles affects the phonon distribution. Since the quasiparticle density is larger than in equilibrium, this leads to a phonon occupation probability bigger than the equilibrium probability, as captured by the term $n_2(\omega)$ in Eq. (44) (see also Appendix C, where we give an expression for n_2 valid up to $\omega \simeq 2\Delta + T_*$; the analytically calculated phonon distribution is in good agreement with the numerical results).

In Fig. 5 the quasiparticle density is shown as a function of T_* for a few different bath temperatures T_B and as a function of T_B for a few different phonon numbers (T_*). The analytical and numerical approaches give consistent

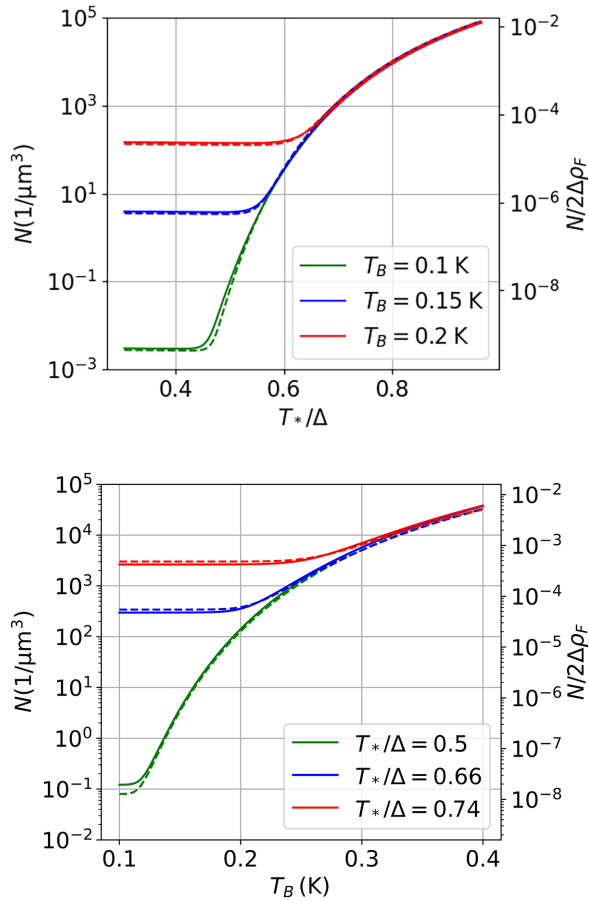


FIG. 5. Quasiparticle densities calculated from the simulation (solid lines) and from solving Eq. (47) in the steady state (dashed lines). The upper plot is obtained by varying the photon number for three different bath temperatures, and the lower plot is obtained by varying the bath temperature for $\bar{n} = 10^7$, 5×10^7 , and 10^8 , respectively. The thermalization time is fixed at $\tau_l = \tau_0^{\text{PB}}$, and the other parameters are as in Fig. 3 (given in Table I). The corrections to the leading analytical results given in Appendix E are included.

results over a range of parameter values relevant to experiments, with small deviations arising at low temperatures and photon numbers. These deviations are caused by the condition $\omega_0 \ll T_*$ holding only weakly, and we checked that there is a closer match between the two approaches when decreasing the photon energy. For $\bar{n} \gg 1$, Eq. (14) is a symmetric function of ω_0 ; therefore, the leading corrections to Eq. (19) and hence to the density are of order $(\omega_0/T_*)^2$. As the magnitude of the deviations is beyond the accuracy of the considerations in the next section, we do not pursue this further.

In Fig. 6 the nonequilibrium gap suppression $\delta\Delta$, Eq. (53), is compared with the equilibrium one $\delta\Delta_T$ for the same set of parameters as in Fig. 5. Superconductivity is enhanced relative to that in thermal equilibrium when the difference $\delta\Delta_T - \delta\Delta$ is positive. We focus on the region of low photon number (relatively small T_*/Δ), where the enhancement occurs; in this region the factor in square brackets in Eq. (53) gives the main dependence of the gap on photon number, causing the gap to increase compared with the gap in thermal equilibrium. For larger photon numbers the quasiparticle density increases quickly (see Fig. 5), leading to a strong suppression of the gap since $\delta\Delta \propto N_{\text{QP}}$. The analytical estimate (dashed lines) slightly overestimates the enhancement compared with the numerical results (solid lines), but both sets of curves display a maximum at the temperature-dependent value of T_* at which $G(T_*/\Delta)$ becomes the dominant term in Eq. (47); that is, above this value, quasiparticle creation from reabsorption of pair-breaking phonons becomes dominant.

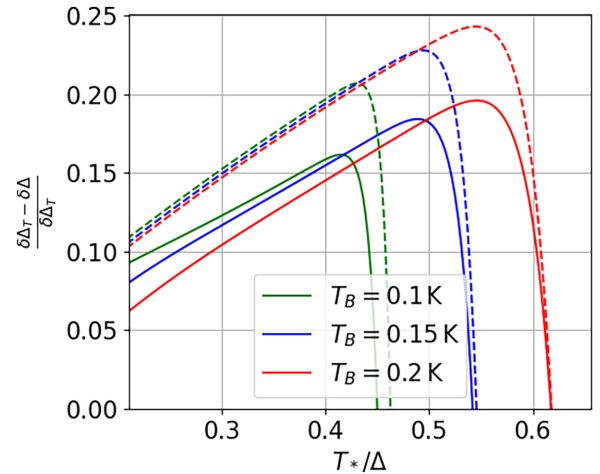


FIG. 6. Suppression $\delta\Delta$ of the gap as function of T_* for the same parameters used in the upper panel in Fig. 5. Solid lines are numerical results, and dashed lines correspond to the analytical formula in Eq. (53). The suppression is compared with that in thermal equilibrium, $\delta\Delta_T$; a positive difference $\delta\Delta_T - \delta\Delta$ corresponds to gap enhancement. The rapid change from positive to negative coincides with the onset of large nonequilibrium quasiparticle density (see Fig. 5).

V. QUALITY FACTOR AND RESONANCE FREQUENCY

The ac response of a superconductor depends on the quasiparticle distribution function, and the dissipative part can be strongly affected under nonequilibrium conditions; see, for example, Ref. [29]. Indeed, the real part σ_1 of the ac conductivity $\sigma = \sigma_1 + i\sigma_2$ at frequency ω_0 is given by

$$\sigma_1 = \frac{2\sigma_N}{\omega_0} \int_{\Delta}^{\infty} dE [f(E) - f(E + \omega_0)] \times \rho(E) U^+(E, E + \omega_0). \quad (54)$$

To estimate σ_1 , we can use the low-energy approximation for coherence factors and density of states [see Eq. (21)], expand the integrand in Eq. (54) to lowest order in ω_0 , and use the numerical result $\int_0^{\infty} dx f'(x)/x \simeq -1.15b_0$, where $x = (E - \Delta)/T_*$, to find

$$\sigma_1 \simeq 2.3\sigma_N \frac{\Delta}{T_*} b_0 \simeq 0.77\sigma_N \frac{N_{\text{QP}}}{2\rho_F \Delta} \left(\frac{\Delta}{T_*}\right)^{3/2}. \quad (55)$$

The form on the right shows that the dependence of σ_1 on the distribution function is not only via proportionality to the quasiparticle density, due to the appearance of T_* in the last factor. Interestingly, as T_* increases (at fixed N_{QP}), dissipation decreases; this effect is due to the redistribution of quasiparticles to higher energies, where the density of states is lower, similar to the decrease in relaxation of a superconducting qubit in which a residual quasiparticle is pushed on average to higher energy in the presence of a microwave drive [30].

For $(\omega_0/4\Delta)^2 \ll 1$, the imaginary part σ_2 can be approximated as $\sigma_2 \simeq (\pi\sigma_N\Delta_0)/\omega_0 + \delta\sigma_2$, with

$$\begin{aligned} \delta\sigma_2 &= -\delta\sigma_{2,f} - \delta\sigma_{2,\Delta}, \\ \delta\sigma_{2,f} &= \frac{2\sigma_N}{\omega_0} \int_{\Delta-\omega_0}^{\Delta} dE f(E + \omega_0) \frac{U^+(E, E + \omega_0)E}{\sqrt{\Delta^2 - E^2}}, \\ \delta\sigma_{2,\Delta} &= \frac{\pi\sigma_N\delta\Delta}{\omega_0}. \end{aligned} \quad (56)$$

The contribution $\delta\sigma_2$ collects all the quasiparticle effects, with $\delta\sigma_{2,f}$ accounting directly for their distribution and $\delta\sigma_{2,\Delta}$ being due to the gap suppression of Eq. (52). Calculation of $\delta\sigma_{2,f}$ requires knowledge of the shape of the distribution function within the first peak above the gap, and it is therefore beyond the description in terms of only the envelope that we use in our analytical approach. For this reason, this term is evaluated numerically in what follows. Still, we can give an order-of-magnitude estimate assuming $f \sim b_0$, which gives $\delta\sigma_{2,f} \sim 2\pi\sigma_N\Delta_0 b_0/\omega_0$; this shows that the two contributions to $\delta\sigma_2$ can be of similar magnitude.

Knowledge of the ac conductivity makes it possible to estimate the internal quality factor Q_i and the resonance-frequency shift $\delta\omega_0$ of superconducting resonators. For half-wavelength, open-ended resonators made of thin superconducting film, we have [31,32]

$$Q_i = \frac{\sigma_2}{\alpha\sigma_1} \simeq \frac{\sigma_N\pi\Delta_0}{\omega_0\alpha\sigma_1} \simeq \frac{\pi T_*}{2.3\alpha\omega_0 b_0}, \quad (57)$$

where α is the kinetic inductance fraction (that is, the ratio between kinetic inductance and total inductance of the resonator) and

$$\frac{\delta\omega_0}{\omega_0} = \frac{\alpha}{2} \frac{\delta\sigma_2}{\sigma_2} \simeq -\frac{\alpha\delta\Delta}{2\Delta_0} - \frac{\alpha\omega_0\delta\sigma_{2,f}}{2\pi\sigma_N\Delta_0}. \quad (58)$$

Not surprisingly, this expression resembles that for the frequency shift in superconducting qubits, in which terms originating from gap suppression and virtual transitions mediated by quasiparticle tunneling have been identified [33]. Note that, in contrast to the frequency shift, the first peak's shape does not affect the calculation of Q_i , since $\delta\sigma_2/\sigma_2 \ll 1$.

Both the quality factor and the frequency shift depend, in general, on the bath temperature T_B and the photon number \bar{n} through b_0 and T_* [in particular, the quality factor scales inversely with quasiparticle density, see Eq. (41), but it also depends explicitly on T_*]. For comparison with experiments, we henceforth assume that T_B corresponds to the reported base temperature of the fridge. To estimate \bar{n} , we relate it to power absorbed by the quasiparticles P_{abs} :

$$\bar{n} = \frac{Q_i P_{\text{abs}}}{\omega_0^2}. \quad (59)$$

Using this relation in Eq. (57), we arrive at an implicit equation for Q_i in terms of P_{abs} . The latter is, in general, not a directly measurable quantity; however, for a half-wavelength resonator capacitively coupled to a transmission line, we follow Ref. [13] and relate P_{abs} to the readout power P_{read} :

$$P_{\text{abs}} = 2P_{\text{read}} \frac{Q^2}{Q_i Q_c}, \quad (60)$$

where $Q = Q_i Q_c / (Q_i + Q_c)$ is the loaded quality factor and Q_c is the coupling quality factor. The same expression for \bar{n} in terms of P_{read} is obtained with use of the relation between internal power and photon number, $P_{\text{int}} = \bar{n}\omega_0^2/2\pi$, together with that between internal and readout powers, $P_{\text{int}} = P_{\text{read}} Q^2 / \pi Q_c$ [31]. Equations (57), (59), and (60) make possible a self-consistent calculation of the photon number and the internal quality factor as a function of readout power. In the following, we solve these equations explicitly in two regimes.

The approach just described is simplified considerably in the limit $Q_i \gg Q_c$, in which Eqs. (59) and (60) reduce to $\bar{n} = 2Q_c P_{\text{read}}/\omega_0^2$, which is independent of Q_i . Then T_* can be calculated from its definition, Eq. (24), and b_0 by solving Eq. (45). In what follows, we denote with $T_{*,0}$ the value of T_* obtained under the assumption $Q_i \gg Q_c$, namely,

$$\frac{T_{*,0}}{\Delta} \equiv \left[\frac{105}{64} \left(\frac{T_c}{\Delta} \right)^3 c_{\text{phot}}^{\text{QP}} \tau_0 \frac{2P_{\text{read}}Q_c}{\Delta^2} \right]^{1/6}. \quad (61)$$

If we further consider the regime of low phonon temperature and high photon number, $T_B \ll T_B^*$, we find that the quality factor is given by

$$Q_{i,0} = \frac{\gamma_0 \Delta \tau_0^{\text{PB}}}{\alpha \omega_0 \tau_l} \left(\frac{\Delta}{T_{*,0}} \right)^3 e^{\sqrt{14/5}(\Delta/T_{*,0})^3}, \quad (62)$$

with $\gamma_0 = \pi 2^{1/3} 5 \sqrt{7} (2.1)^2 / (2.3 \times 3^{3/2}) \simeq 19.3$. Therefore, in this case the quality factor is a decreasing function of readout power and does not depend on T_B . The fast decrease of the quality factor with increasing power is due to the large increase in the number of quasiparticles with increasing photon number, as discussed in Sec. IV A.

The regime of high phonon temperature and low photon number, $T_B \gtrsim T_B^*$, also offers significant simplification, since in that case we can relate b_0 to the (thermal) quasiparticle density using Eq. (41), and rewrite Eq. (57) as

$$Q_i = \frac{2.1\sqrt{2}\pi}{2.3\alpha} \frac{\Delta}{\omega_0} \left(\frac{T_*}{\Delta} \right)^{3/2} \left(\frac{N_{\text{QP}}^{T_B}}{2\rho_F \Delta} \right)^{-1} \quad (63)$$

where the superscript T_B in $N_{\text{QP}}^{T_B} = 2\rho_F \Delta \sqrt{2\pi T_B/\Delta} e^{-\Delta/T_B}$ denotes the thermal-equilibrium density at temperature T_B , which is independent of \bar{n} . This formula, with use of Eqs. (24), (59) and (60), leads to a quadratic equation for Q_i whose solution can be written in the form

$$Q_i = \sqrt{\left(\frac{Q_c}{2} \right)^2 + \left(\frac{2.1\sqrt{2}\pi \Delta}{2.3\alpha \omega_0} \right)^2 \left(\frac{T_{*,0}}{\Delta} \right)^3 \left(\frac{N_{\text{QP}}^{T_B}}{2\rho_F \Delta} \right)^{-2}} - \frac{Q_c}{2}. \quad (64)$$

In this regime, Q_i is an increasing function of readout power (through $T_{*,0}$) and depends exponentially on T_B (through $N_{\text{QP}}^{T_B}$). As remarked above, the increase of the quality factor with readout power can be traced to the redistribution of the quasiparticles to higher energies, where the density of states is lower. Note that if $Q_i \gg Q_c$ holds up to temperatures of order T_B^* or higher, Eqs. (62) and (64) together capture the temperature and power dependence of Q_i at all temperatures; we do not investigate here the case in which this condition is not satisfied.

So far we have assumed that the internal quality factor is determined by the energy absorbed by quasiparticles. More generally, extrinsic (i.e., nonquasiparticle) mechanisms such as dielectric losses can contribute to the total internal quality factor $Q_{i,\text{tot}}$; collecting those contributions into $Q_{i,\text{ext}}$ we have

$$1/Q_{i,\text{tot}} = 1/Q_i + 1/Q_{i,\text{ext}}, \quad (65)$$

where, as before, Q_i denotes the quasiparticle part. For $T_B \gtrsim T_B^*$, Q_i is given by Eq. (64) with the replacement $1/Q_c \rightarrow 1/Q_c + 1/Q_{i,\text{ext}}$ and is therefore unchanged (at leading order) if $Q_{i,\text{ext}} \gg Q_c$.

We now proceed to compare our theoretical findings with the measurements of the temperature dependencies of the quality factor and the resonance frequency for different readout powers reported in Ref. [13]. In that work, a temperature-independent plateau in the quality factor at low temperatures is observed, which qualitatively agrees with the result in Eq. (62). By comparing experimental values with numerical calculations, de Visser *et al.* [13] suggest the plateau is explainable by the nonequilibrium steady-state solution to the kinetic equations. However, estimating the value of the plateau $Q_{i,0}$, Eq. (62), using the parameters in Table II, we find much-larger values than measured experimentally (see Table III). The discrepancy cannot be due to approximations being used: while in particular the assumption $\omega_0 \ll T_*$ holds only weakly, for the highest readout power comparison with numerical results (see Fig. 5) shows that our analytical expression underestimates the quasiparticle density by a factor smaller than 2; then the quality factor could be overestimated by the same factor, but the estimated quality factor is 3 orders of magnitude larger than the measured quality factor [34]. This indicates that the plateau is not due to the quasiparticles being driven out of equilibrium by the resonator's photons, but is due to some other driving mechanism and/or extrinsic relaxation channels. The measured power dependence of the quality factor is qualitatively opposite that typically expected in the presence of two-level systems [35], so they are unlikely to be the cause of the plateau. Moreover, the low-temperature saturation of the quasiparticle

TABLE II. Parameters used for comparison between theory in this work and experiments in Ref. [13]. The estimation of $c_{\text{phot}}^{\text{QP}}$, Δ_0 , and α is discussed in Appendix F. For the phonon thermalization time τ_l and the coupling quality factor $Q_c = 20\,100$, we use the same values as in Ref. [13]. In the numerical calculations, the gap is fixed at its thermal-equilibrium value Δ_T , the discretization step size $h = \Delta_T/189$, and the energy is truncated at $E_{\text{max}} = 10\Delta_T$. The time τ_0 is used as a free fit parameter, while τ_0^{PB} follows from it via Eq. (13).

$c_{\text{phot}}^{\text{QP}}$	τ_0	Δ_0	ω_0	τ_0^{PB}	τ_l	α
0.06 Hz	63 ns	189 μeV	$22\Delta_T/189$	40 ps	170 ps	0.13

TABLE III. For each readout power used in Ref. [13], we calculate $T_{*,0}$ using Eq. (61) and the (theoretical) low-temperature quality factors $Q_{i,0}$ using Eq. (62) (except for the lowest power, since in that case $T_{*,0} \simeq \omega_0$, while the theory is valid for $T_{*,0} > \omega_0$). The experimental low-temperature quality factors $Q_{i,\text{ext}}$ are assumed to be due to extrinsic (nonquasiparticle) mechanisms (see the main text).

P_{read} (dBm)	−100	−90	−80	−72	−68	−64
$T_{*,0}/\Delta$	0.12	0.18	0.26	0.36	0.42	0.49
$Q_{i,0}/10^6$		10^{124}	10^{38}	10^{13}	10^7	10^3
$Q_{i,\text{ext}}/10^6$	2.5	2.5	2.5	1.3	0.9	0.7

lifetime reported in Ref. [13] (for a different sample and for a narrower range of power) points to the presence of a second driving mechanism, a situation that deserves further study. Nonetheless, assuming for simplicity an extrinsic mechanism, we use Eq. (65) to fit the experimental data and find the values of $Q_{i,\text{ext}}$ given in Table III. Results obtained with the analytical formula and from the numerical calculations are compared with experimental data for the quality factor and the resonance frequency in Fig. 7; in the numerical calculations, the experimentally measured (total) internal quality factor is used in Eqs. (59) and (60) to obtain the photon number. At temperatures $T \gtrsim 0.25$ K we find good agreement between theory and experiment. The fitted value of τ_0 is less than an estimate derived from neutron-scattering data [21] but is consistent with other experimental estimates; see for example, Ref. [36]. This further validates our approach, especially since from the analytical expressions it is evident that τ_0 enters into the quality factor via the product $c_{\text{phot}}^{\text{QP}} \tau_0 \bar{n}$, and therefore

inaccuracies in the estimates of $c_{\text{phot}}^{\text{QP}}$ and/or \bar{n} (equivalently, P_{read}) could affect the extracted value of τ_0 .

The disagreement between theory and experiment for the frequency shift at low temperature and readout power greater than -80 dBm could perhaps be due to the same driving and/or extrinsic mechanisms responsible for the saturation of the low-temperature quality factor. It is suggested in Ref. [37] that the depairing effect of a microwave drive modifies the density of states in such a way to cause a negative frequency shift proportional to the power; however, the corresponding influence on the quality factor was not analyzed. Finally, we note that in agreement with the discussion after Eq. (56), on the basis of our numerical calculations about 40%–45% of the calculated frequency shift originates from the gap suppression, which is comparable to the direct contribution due to the nonequilibrium distribution.

VI. SUMMARY

In this work we investigate the quasiparticle distribution function in superconducting resonators in the regime of low quasiparticle density in the presence of a large number of low-energy ($\omega_0 \ll \Delta$) photons and of a low-temperature ($T_B \ll \Delta$) phonon bath. In the steady state, we present approximate analytical solutions to the kinetic equations governing the dynamics of the quasiparticle and phonon distribution functions. The shape of the quasiparticle distribution function—that is, its functional dependence on energy—is determined by interplay between absorption and emission of photons and phonons (see Sec. III) and has a typical width T_* above the gap [see Eq. (24) and Ref. [30]]. The overall normalization and hence the

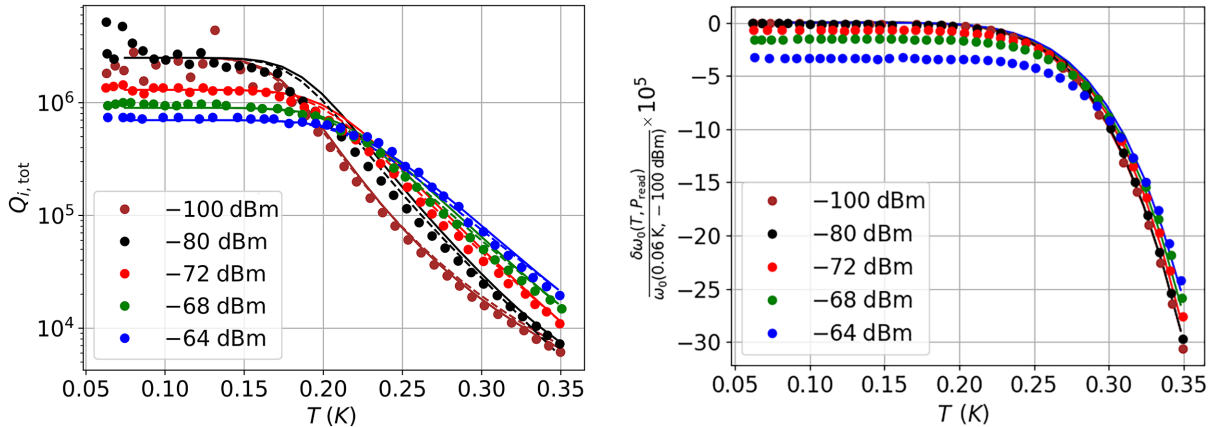


FIG. 7. Internal quality factor $Q_{i,\text{tot}}$ versus temperature for different readout powers (left) and deviation of the resonance frequency from its experimentally determined low-temperature and low-readout-power value $\delta\omega_0(T, P_{\text{read}}) = \omega_0(T, P_{\text{read}}) - \omega_0(T = 0.06 \text{ K}, P_{\text{read}} = -100 \text{ dBm})$ in the unit of $10^{-5}\omega_0$ for different readout powers (right). Experimental data from [13] are displayed as circles (we omit the data for $P_{\text{read}} = -90$ dBm for clarity of presentation), results from the numerical calculations described in Sec. II C are displayed as solid lines, and results from the analytical formulas [Eqs. (62)–(65)] are displayed as dashed lines. The analytical curve for the lowest readout power assumes thermal equilibrium (see Appendix F).

quasiparticle density are controlled by the balance between recombination by phonon emission and generation (see Sec. IV); due to the photons driving the quasiparticles out of equilibrium, the generation is due not only to thermal phonons but also to nonequilibrium phonons emitted by quasiparticles of sufficiently high energy. The density dynamics then follows from the generalized Rothwarf-Taylor model in Sec. IV A; for $T_B > T_B^* = T_*^3/\Delta^2$, the steady-state density is approximately the same as in thermal equilibrium, while it is much larger than that at lower bath temperatures. The analytical results are validated by comparison with numerical calculations.

Our results enable us to calculate the dependence on temperature and readout power of the internal quality factor and (numerically) of the frequency shift in thin-film resonators (see Sec. V). In contrast to previous suggestions [12,13], we find that the quasiparticle distribution driven out of equilibrium by the resonator's photons cannot explain the experimental data in Ref. [13] at low temperature, while it quantitatively describes them above about 0.25 K (see Fig. 7).

ACKNOWLEDGMENTS

We gratefully acknowledge D. Basko for interesting discussions. This work was supported in part by the German Federal Ministry of Education and Research (BMBF), funding program ‘‘Quantum Technologies—From Basic Research to Market,’’ project QSolid (Grant No. 13N16149). G.C. acknowledges support by the U.S. Government under ARO grant W911NF2210257.

APPENDIX A: QUASIPARTICLE AND PHONON LIFETIMES

In Sec. IID a number of lifetimes are introduced to qualitatively discuss the behavior of the quasiparticle distribution function out of equilibrium. Here we give their precise definitions in terms of the nonequilibrium quasiparticle and phonon distributions, as obtained by our inspecting the structure of the kinetic equations. As in Sec. IID, we consider first the phonon lifetimes.

The lifetime of a phonon of energy ω with regard to pair breaking is given by [see the last term in curly brackets in the second integral in Eq. (12)]

$$\frac{1}{\tau_{\text{PB}}^{\text{phon}}(\omega)} = \frac{1}{\pi \Delta_0 \tau_0^{\text{PB}}} \int_{\Delta}^{\omega-\Delta} dE \rho(E) U^+(E, \omega - E) \times [1 - f(\omega - E)][1 - f(E)]. \quad (\text{A1})$$

Approximating the Pauli-blocking factors as $[1 - f(E)] \simeq 1$, as done throughout this paper, we can express the dependence of $1/\tau_{\text{PB}}^{\text{phon}}$ on ω in terms of the spectral density S_+

in Refs. [38,39] as

$$\frac{1}{\tau_{\text{PB}}^{\text{phon}}(\omega)} = \frac{\Delta}{\pi \Delta_0 \tau_0^{\text{PB}}} S_+(\omega/\Delta), \quad (\text{A2})$$

where

$$S_+(x) = (x+2)E \left(\frac{x-2}{x+2} \right) - \frac{4x}{x+2} K \left(\frac{x-2}{x+2} \right), \quad (\text{A3})$$

with E and K the complete elliptic integrals of the second and first kind, respectively. Note that $S_+(x) = 0$ for $x < 2$, $S_+(x) \simeq x$ for $x \gg 2$, and $S_+(x) \simeq \pi [1 + (x-2)/4]$ for $x-2 \ll 2$. The last expression shows that the pair-breaking lifetime approaches τ_0^{PB} at low temperature and only weakly depends on energy for $\omega \gtrsim 2\Delta$.

The lifetime of a phonon against with regard to being absorbed by a quasiparticle is given by [see the last term in curly brackets in the first integral in Eq. (12)]

$$\frac{1}{\tau_{\text{abs}}^{\text{phon}}(\omega)} = \frac{2}{\pi \Delta_0 \tau_0^{\text{PB}}} \int_{\Delta}^{\infty} dE \rho(E) U^-(E, E + \omega) \times f(E) [1 - f(E + \omega)]. \quad (\text{A4})$$

For $f \ll 1$, one can show that the right-hand side is bounded by $1/\pi \tau_0^{\text{PB}}$ times the normalized quasiparticle density $N_{\text{QP}}/2\rho_F \Delta$. Since at low temperature the latter is much smaller than 1, we have $\tau_{\text{abs}}^{\text{phon}} \gg \tau_0^{\text{PB}}$.

The last phonon lifetime we take into account is the thermalization time τ_l . For a phonon of energy 2Δ whose mean free path with regard to pair breaking $s\tau_0^{\text{PB}}$ (with s the speed of sound) is of a similar order as the film thickness d , τ_l can be estimated to be given by [19,26,27]

$$\tau_l \approx \frac{4d}{\eta s}, \quad (\text{A5})$$

where η is the direction-averaged transmission coefficient between the film and the substrate. For aluminum on sapphire, the speed of sound and the transmission coefficient are $s \simeq 3.3\text{--}6.7$ km/s and $\eta \simeq 0.2$, respectively [26]. For the resonator of Ref. [13] considered in Sec. V, this expression gives $\tau_l \simeq 180\text{--}360$ ps. In Ref. [13], $\tau_l = 170$ ps was used, and to simplify comparison with the results therein, we also use this latter value in our analysis. Our results do not depend on the exact value of the thermalization time at energies $\omega < 2\Delta$ if the condition $\tau_{\text{abs}}^{\text{phon}} \gg \tau_l$ holds, as is the case for both choices of τ_l . We note that some authors [24,40] suggest the thermalization time of phonons with $\omega < 2\Delta$ is limited by total internal reflection and, for sufficiently smooth interfaces, to be several orders of magnitude longer than the thermalization time at energies above 2Δ . We assume this not to be the case and use the thermalization time at energy $\omega = 2\Delta$ for all energies.

We now turn to the quasiparticle lifetimes. The scattering lifetime $\tau_{s,t}^{\text{QP}}$ of a quasiparticle due to interaction with photons has three contributions,

$$\frac{1}{\tau_{s,t}^{\text{QP}}} = \frac{1}{\tau_{\text{sp},t}^{\text{QP}}} + \frac{1}{\tau_{\text{st},t}^{\text{QP}}} + \frac{1}{\tau_{\text{abs},t}^{\text{QP}}}, \quad (\text{A6})$$

originating, respectively, from spontaneous emission, stimulated emission, and absorption of a photon. They are given respectively by [see the second terms in curly brackets in Eq. (14)]

$$\frac{1}{\tau_{\text{sp},t}^{\text{QP}}} = c_{\text{phot}}^{\text{QP}} U^+(E, E - \omega_0) [1 - f(E - \omega_0)], \quad (\text{A7})$$

$$\frac{1}{\tau_{\text{st},t}^{\text{QP}}} = c_{\text{phot}}^{\text{QP}} \bar{n} U^+(E, E - \omega_0) [1 - f(E - \omega_0)], \quad (\text{A8})$$

$$\frac{1}{\tau_{\text{abs},t}^{\text{QP}}} = c_{\text{phot}}^{\text{QP}} \bar{n} U^+(E, E + \omega_0) [1 - f(E + \omega_0)]. \quad (\text{A9})$$

The scattering lifetime $\tau_{s,n}^{\text{QP}}$ due to interaction with phonons also has three contributions,

$$\frac{1}{\tau_{s,n}^{\text{QP}}} = \frac{1}{\tau_{\text{sp},n}^{\text{QP}}} + \frac{1}{\tau_{\text{st},n}^{\text{QP}}} + \frac{1}{\tau_{\text{abs},n}^{\text{QP}}}, \quad (\text{A10})$$

accounting for spontaneous phonon emission [see the last term in curly brackets in Eq. (5)]

$$\frac{1}{\tau_{\text{sp},n}^{\text{QP}}} = \frac{1}{\tau_0 T_c^3} \int_0^{E-\Delta} d\omega \omega^2 U^-(E, E - \omega) [1 - f(E - \omega)], \quad (\text{A11})$$

stimulated phonon emission [see the last term in curly brackets in the second integral in Eq. (8)]

$$\begin{aligned} \frac{1}{\tau_{\text{st},n}^{\text{QP}}} &= \frac{1}{\tau_0 T_c^3} \int_0^{E-\Delta} d\omega \omega^2 U^-(E, E - \omega) n(\omega) \\ &\times [1 - f(E - \omega)], \end{aligned} \quad (\text{A12})$$

and phonon absorption [see the last term in curly brackets in the first integral of Eq. (8)]

$$\begin{aligned} \frac{1}{\tau_{\text{abs},n}^{\text{QP}}} &= \frac{1}{\tau_0 T_c^3} \int_0^\infty d\omega \omega^2 U^-(E, E + \omega) n(\omega) \\ &\times [1 - f(E + \omega)]. \end{aligned} \quad (\text{A13})$$

In addition, the lifetime of a quasiparticle with regard to recombination is given by [see Eq. (10)]

$$\begin{aligned} \frac{1}{\tau_r^{\text{QP}}} &= \frac{1}{\tau_0 T_c^3} \int_{E+\Delta}^\infty d\omega \omega^2 U^+(E, \omega - E) \\ &\times f(\omega - E) [1 + n(\omega)]. \end{aligned} \quad (\text{A14})$$

For a system in equilibrium, these lifetimes (except those due to photons) are discussed in Ref. [21]. When $f \ll 1$, the only lifetimes with significant dependence on the quasiparticle distribution function are $\tau_{\text{abs}}^{\text{phon}}$ and τ_r^{QP} : since the rates are proportional to f , the times are inversely proportional to the quasiparticle density. In Appendix E we study the dependence of the recombination coefficient R [i.e., the recombination rate for the quasiparticle density; see Eq. (47)] on T_* , while as discussed in Sec. III C, the effect of $\tau_{\text{abs}}^{\text{phon}}$ on the quasiparticle distribution can be ignored.

APPENDIX B: FINITE PHONON TEMPERATURE

Here we present in some detail the derivation of the results discussed in Sec. III B. As mentioned there, we want to find the energy E_* below which ignoring the effect of thermal phonons is justified, in which case the formulas in Sec. III A can be used, and to find E_* we need an estimate for $\text{St}_{\text{st}}^{\text{phon}}$, Eq. (8), at $E = E_*$. In the integrands in that equation, we assume as usual $f \ll 1$ at all energies; then as long as factors other than $n(\omega) = n_T(\omega, T_B)$ grow with ω more slowly than exponentially, the integral is determined by the integration in the interval around $\omega \sim T_B$. This is the case for all terms except that proportional to $f(E_* - \omega)$, which increases faster than exponentially; for this term, the integral can be estimated as follows: We consider a frequency ω_* such that $\omega_* \gg T_B$ and $\omega_M - \omega_* \gg \tilde{T}_*$, with $\omega_M \gg T_B$ to be defined below (here we assume $E_* \gtrsim 2\Delta$; for $E_* \lesssim 2\Delta$ the condition reads $\omega_M - \omega_* \gg T_*$, with ω_M having different definitions in the two cases). The contribution to the integral from the interval $0 < \omega < \omega_*$ can be estimated together with the other terms in Eq. (8), while that from $\omega_* < \omega < E_* - \Delta$ is to be considered separately.

We start with the low-frequency contribution, $\omega < \omega_*$, which we denote by $\text{St}_{\text{st,low}}^{\text{phon}}$. Then since n restricts ω to be of order $T_B \ll E_*$, while the (envelope of the) quasiparticle distribution function f varies at most over a scale $T_* \gg T_B$, we can approximate $U^-(E_*, E_* \pm \omega) \simeq 1$, perform a series expansion for the distribution functions, and push the integration limit from ω_* to infinity to find

$$\text{St}_{\text{st,low}}^{\text{phon}} \simeq \frac{1}{\tau_0 T_c^3} \int_0^\infty d\omega \omega^4 \frac{\partial^2 f}{\partial E^2} \Big|_{E=E_*} n(\omega, T_B). \quad (\text{B1})$$

According to Eq. (31), for $(E_* - \Delta)/\tilde{T}_* \gg 1$ we have

$$\frac{\partial^2 f}{\partial E^2} \Big|_{E=E_*} \simeq \frac{1}{\tilde{T}_*^2} \left(\frac{E_* - \Delta}{\tilde{T}_*} \right)^3 f(E_*), \quad (\text{B2})$$

and therefore

$$\text{St}_{\text{st,low}}^{\text{phon}} \simeq \frac{24\zeta(5)}{\tau_0 T_c^3} \left(\frac{T_B}{\tilde{T}_*} \right)^5 (E_* - \Delta)^3 f(E_*), \quad (\text{B3})$$

with ζ denoting the Riemann ζ function. From comparison of this expression with Eq. (34), it is clear that the low-frequency contribution can be ignored for $T_B \ll \tilde{T}_*$. A similar calculation for the case $E_* \lesssim 2\Delta$ is slightly more complex, as one needs to use the approximation in Eq. (22) for U^- ; the resulting condition reads $(E_* - \Delta)T_B^5/T_*^6 \ll 1$.

We now turn to the high-frequency contribution

$$\text{St}_{\text{st,hi}}^{\text{phon}} \approx \frac{1}{\tau_0 T_c^3} \int_{\omega_*}^{E_* - \Delta} d\omega \omega^2 f(E_* - \omega) e^{-\omega/T_B}, \quad (\text{B4})$$

where the approximations used are $U^- \approx 1$ and $n(\omega, T_B) \approx e^{-\omega/T_B}$. For $E_* - \omega > 2\Delta$, we can use Eq. (31) for f and estimate the integral using Laplace's method; indeed, the argument of the exponential has a maximum at frequency $\omega_M = E_* - \Delta - \tilde{T}_*(\tilde{T}_*/T_B)^{2/3}$, and $E_* - \omega_M > 2\Delta$ if $T_B/\Delta < (T_*/\Delta)^3$. Similarly, for $E_* - \omega < 2\Delta$ one can use the asymptotic approximation for the result in Eq. (25b) to find $\omega_M = E_* - \Delta - T_*(T_*/T_B)^{1/2}$, and $E_* - \omega_M < 2\Delta$ if $(T_*/\Delta)^3 < T_B/\Delta \ll T_*/\Delta$ [we note that the algebraic prefactor is different in this case, as U^- takes approximately the form given in Eq. (22)]. The estimate of the integral in Eq. (B4) is then obtained by our evaluating the prefactor at $\omega = \omega_M$, expanding the argument of the exponential up to second order around ω_M , and finally evaluating the resulting Gaussian integral; here the integration limits can be extended to infinity, since the width of the Gaussian peak is of order $\tilde{T}_*(T_B/\tilde{T}_*)^{1/6}$ for $E_* > 2\Delta$ and $T_*(T_B/T_*)^{1/4}$ for $E_* < 2\Delta$.

We can now use the estimate thus found for $\text{St}_{\text{st}}^{\text{phon}}$ in Eq. (33) together with Eq. (34) to arrive at the following equation for $E_* > 2\Delta$:

$$4\sqrt{3\pi}(\tilde{x}_* - \tilde{\chi}^{2/3})^2 e^{(3/5)\tilde{\chi}^{5/3} + (2/5)\tilde{x}_*^{5/2} - \tilde{\chi}\tilde{x}_*} = \tilde{x}_*^{9/4} \tilde{\chi}^{2/3}, \quad (\text{B5})$$

where $\tilde{x}_* = (E_* - \Delta)/\tilde{T}_*$ and $\tilde{\chi} = \tilde{T}_*/T_B$. For $E_* < 2\Delta$, the term St^{phot} in Eq. (33) can be expressed as the opposite of the first term on the right-hand side of Eq. (23), and we similarly find the equation

$$105\sqrt{\pi}(x_* + \sqrt{\chi})(x_* - \sqrt{\chi})^2 e^{(2/3)\chi^{3/2} + (1/3)x_*^3 - x_*\chi} = 64x_*^3 \chi^{3/4}, \quad (\text{B6})$$

with $x_* = (E_* - \Delta)/T_*$ and $\chi = T_*/T_B$. These equations can be solved approximately by expansion up to second order, both in the prefactors and in the argument of the exponential, around $\tilde{x}_* = \tilde{\chi}^{2/3}$ ($x_* = \sqrt{\chi}$), to find for

$$T_B \ll T_B^*$$

$$E_* \simeq \Delta + \tilde{T}_*(\tilde{T}_*/T_B)^{2/3} + \tilde{T}_* \sqrt{\frac{4}{3} \left(\frac{T_B}{\tilde{T}_*}\right)^{1/3} W \left[\frac{\sqrt{3}}{16\sqrt{\pi}} \left(\frac{\tilde{T}_*}{T_B}\right)^{5/2} \right]} \gtrsim 2\Delta, \quad (\text{B7})$$

where W is the Lambert or product logarithm function with the asymptotic behavior $W(x) \simeq \ln x - \ln \ln x$ for $x \gg 1$, while for $T_B^* \lesssim T_B \ll T_*$ we get

$$E_* \simeq \Delta + T_*(T_*/T_B)^{1/2} + T_* \sqrt{\left(\frac{T_B}{T_*}\right)^{1/2} W \left[\frac{32}{105\sqrt{\pi}} \left(\frac{T_*}{T_B}\right)^{9/4} \right]} \lesssim 2\Delta. \quad (\text{B8})$$

In Sec. III B we report for simplicity only the leading terms for E_* .

By construction, the energy E_* denotes that energy at which the effects of absorption and stimulated emission of phonons become comparable to the effect of photons, so ignoring $\text{St}_{\text{st}}^{\text{phon}}$ is justified only below E_* . Conversely, we now show that for $E > E_*$ we can ignore the photons, and the quasiparticle distribution function takes the Boltzmann form,

$$f(E) \propto e^{-E/T_B}. \quad (\text{B9})$$

It is straightforward to check that (within the approximation of ignoring the Pauli-blocking factors) this form satisfies the equation

$$\text{St}_{\text{sp}}^{\text{phon}} \{f\} + \text{St}_{\text{st}}^{\text{phon}} \{f, n_T\} = 0. \quad (\text{B10})$$

Then using this equation and Eq. (27), which is valid irrespective of the exact form of f , we can write

$$\text{St}_{\text{st}}^{\text{phon}} \simeq \text{St}_{\text{sp}}^{\text{phon}} \Big|_{E=E_*} \left(\frac{E - \Delta}{E_* - \Delta} \right)^3 e^{-(E-E_*)/T_B}. \quad (\text{B11})$$

Moreover, using Eq. (B9), we can write the photon collision integral in the form

$$\text{St}_{\text{st}}^{\text{phot}} = \text{St}_{\text{sp}}^{\text{phot}} \Big|_{E=E_*} e^{-(E-E_*)/T_B}. \quad (\text{B12})$$

Since $\text{St}_{\text{st}}^{\text{phot}}|_{E=E_*} = \text{St}_{\text{sp}}^{\text{phon}}|_{E=E_*}$, comparing the last two equations, we see that, $\text{St}_{\text{st}}^{\text{phot}} < \text{St}_{\text{st}}^{\text{phon}}$ for $E > E_*$. Note that to get the estimate in Eq. (B11), we assume the validity of Eq. (B9) at all energies, including $E < E_*$, and this

assumption underestimates the contribution to $\text{St}_{\text{st}}^{\text{phon}}$ from the term in Eq. (8) proportional to $f(E - \omega)$ originating from the interval $E - E_* < \omega < E - \Delta$. However, this contribution is smaller than that coming from the interval $0 < \omega < E - E_*$ if $E - E_* \gtrsim E_* - \Delta - \tilde{T}_*(\tilde{T}/T_B)^{2/3}$ [with E_* in Eq. (B7)], an inequality that identifies the width of the crossover region between the approximate expressions valid below and above E_* . These considerations are for the case $E_* > 2\Delta$, but they can be extended to the interval $E_* < E < 2\Delta$ in the remaining case.

APPENDIX C: NONEQUILIBRIUM PHONON DISTRIBUTION

Here we study the nonequilibrium form of the phonon distribution function. We start by considering energies below the pair-breaking threshold, $\omega < 2\Delta$. Then if we write $n = n_T + n_1$, in the steady state Eq. (12) takes the form (ignoring as usual Pauli-blocking factors)

$$n_1(\omega) = \frac{2\tau_l}{\pi\Delta_0\tau_0^{\text{PB}}} \int_{\Delta}^{\infty} dE \rho(E) U^-(E, E + \omega) \times \left\{ f(E + \omega) [1 + n_T(\omega) + n_1(\omega)] - f(E) [n_T(\omega) + n_1(\omega)] \right\}. \quad (\text{C1})$$

To solve this equation approximately, we consider two limiting cases. First, we consider energies such that $n_1 \ll n_T$; then we can ignore n_1 on the right-hand side, and the resulting expression amounts to the first iterative solution. To this case belongs in particular the low-energy regime $\omega \ll T_B$, in which case we can approximate $n_T(\omega) \simeq T_B/\omega$, $f(E + \omega) \simeq f(E) + \omega f'(E)$, $U^-(E, E + \omega) \simeq U^-(E, E) = 1/\rho(E)$ and therefore find $n_1 \simeq (2\tau_l/\pi\tau_0^{\text{PB}})(T_B/\Delta_0)b_0$. Then typically $n_1 \ll n_T$ unless τ_l is several orders of magnitude greater than τ_0^{PB} .

A second limiting case is when $n_T \ll n_1 \ll f(E + \omega)/f(E)$ (since f is, in general, monotonically decreasing, the latter inequality also implies $n_1 \ll 1$). In this case n_1 is approximately as in Eq. (39), and using Eq. (25b), we have, for $T_* \lesssim \omega \lesssim \Delta$,

$$f(E + \omega) \simeq \frac{3b_0}{2^{5/6}\sqrt{\pi}} \left(\frac{E + \omega - \Delta}{T_*} \right)^{-(1/2)} \times e^{-[(E + \omega - \Delta)/T_*]^3/3}. \quad (\text{C2})$$

In the argument of the exponential function, we can keep terms linear in $(E - \Delta)/T_*$ while disregarding higher powers, and for $\omega \gtrsim T_*$ we can approximate $U^-(E, E + \omega) \simeq \omega/\sqrt{\omega^2 + 2\omega\Delta}$. In calculating the integral over energy E in Eq. (C1), we can also approximate $\rho(E) \simeq$

$\sqrt{\Delta/(2(E - \Delta))}$ to arrive at

$$n_1(\omega) \simeq \frac{3}{2^{1/3}\pi} b_0 \frac{\tau_l}{\tau_0^{\text{PB}}} \left(\frac{T_*}{\Delta} \right)^2 \frac{\Delta}{\omega} \sqrt{\frac{\Delta}{2\Delta + \omega}} e^{-(\omega/T_*)^3/3}. \quad (\text{C3})$$

For $\omega \gtrsim \Delta$ we can proceed as for $\omega \lesssim \Delta$, but using Eq. (31) instead of Eq. (25b); in this way we obtain

$$n_1(\omega) \simeq \frac{2^{1/6}3^{3/2}}{\sqrt{5}\pi} b_0 \frac{\tau_l}{\tau_0^{\text{PB}}} \left(\frac{T_*}{\Delta} \right)^2 \frac{\Delta}{\omega} \sqrt{\frac{\Delta}{2\Delta + \omega}} \times \exp \left[-\frac{2}{5} \sqrt{\frac{35}{64}} \left(\frac{\omega}{T_*} \right)^{5/2} \sqrt{\frac{\Delta}{T_*}} \right]. \quad (\text{C4})$$

Note that the two exponents in Eqs. (C3) and (C4) match at $\omega = 63\Delta/80$, which as expected is of order Δ .

To find the crossover frequency ω_c between the thermal distribution at $\omega < \omega_c$ and the nonequilibrium distribution at higher energies, assuming $\omega_c \lesssim \Delta$, we equate Eq. (C3) for n_1 to $n_T(\omega) \simeq e^{-\omega/T_B}$, which leads to the equation

$$\frac{1}{3}y^3 - \frac{T_*}{T_B}y + \ln y + \frac{1}{2} \ln \left(1 + \frac{T_*}{2\Delta}y \right) + \ln \left(\frac{2^{5/6}\pi}{3} \frac{\Delta}{T_*} \frac{\tau_0^{\text{PB}}}{\tau_l} b_0^{-1} \right) = 0, \quad (\text{C5})$$

where $y = \omega_c/T_*$. For $y \ll \sqrt{3T_*/T_B}$, we can ignore the first term in this equation, and up to small corrections we arrive at Eq. (40). More-accurate estimates for ω_c can be found by solving Eq. (C5) numerically. For $\omega_c \gtrsim \Delta$, the same approach can be used, but with use of Eq. (C4) for n_1 .

We now turn to energies above the pair-breaking threshold, $\omega > 2\Delta$. On the basis of the considerations thus far, so long as $\omega_c \lesssim 2\Delta$, we expect the inequalities $n_T \ll n_1 \ll 1$ to hold, meaning that we could discard n_T in Eq. (12); however, to allow for $\omega_c > 2\Delta$ we keep the n_T term. In both cases, in the second integral in Eq. (12) we can ignore $n(\omega) \ll 1$ in the first term in curly brackets and, using the approximate energy independence of $1/\tau_{\text{PB}}^{\text{phon}}$ (see Appendix A), we can rewrite the second term as $-n(\omega)/\tau_0^{\text{PB}}$. Furthermore, we assume the quasiparticle density to be sufficiently low for $\tau_{\text{abs}}^{\text{phon}} \gg \tau_{\text{PB}}^0$ to hold, so we can ignore the second term in curly brackets in the first integral in Eq. (12) (see Sec. IID). Then the approximate

solution for the phonon distribution reads

$$\begin{aligned}
n(\omega) &\simeq \frac{1}{\zeta} [n_1(\omega) + n_2(\omega) + n_T(\omega)] \\
&= \frac{\tau_l}{\pi \Delta_0 \tau_0^{\text{PB}} \zeta} \left[2 \int_{\Delta}^{\infty} dE \rho(E) U^-(E, E + \omega) f(E + \omega) \right. \\
&\quad \left. + \int_{\Delta}^{\omega - \Delta} dE \rho(E) U^+(E, \omega - E) f(\omega - E) f(E) \right] \\
&\quad + \frac{1}{\zeta} n_T(\omega), \tag{C6}
\end{aligned}$$

where

$$\zeta = 1 + \tau_l / \tau_0^{\text{PB}} \tag{C7}$$

is the phonon trapping factor [see Eq. (50)]. The first term in the square brackets coincides with n_1 in Eq. (39), but here the prefactor $1/\zeta$ is smaller than unity, since in addition to scattering a new relaxation channel for phonons (i.e., pair breaking) is now available. The second term in square brackets, $n_2(\omega)$, takes into account phonon generation by quasiparticle recombination. Assuming the (envelope of the) quasiparticle distribution to be monotonically decreasing, we can bound this term by $b_0^2 \Delta S_+(\omega/\Delta)$ [with S_+ in Eq. (A3)], which near $\omega = 2\Delta$ is approximately $b_0^2 \Delta \pi$; then, using Eq. (C4) (with the appropriate prefactor), we find that the first term always dominates over the second one at the threshold $\omega = 2\Delta$ if

$$b_0 < (3 \times 2^{1/6} / \sqrt{5\pi}) \zeta (T_*/2\Delta)^2 e^{-\sqrt{35/32}(2\Delta/T_*)^{3/5}}. \tag{C8}$$

Even if n_2 dominates, as discussed in Sec. III C, these nonequilibrium phonons due to quasiparticle recombination could affect the shape of the quasiparticle distribution only at energies $E > 3\Delta$ by contributing to the collision integral $\text{St}_{\text{st}}^{\text{phon}}$, Eq. (8). For $\omega - 2\Delta \lesssim T_*$, one can apply the low-energy approximation to the product of the density of states and the coherence factor and use Eq. (25a) to evaluate approximately the second term in square brackets in Eq. (C6) to find

$$n_2(\omega) \simeq \frac{b_0^2 \tau_l}{\pi (\tau_0^{\text{PB}} + \tau_l)} [\pi - 1.20(\omega - 2\Delta)^{5/2}]. \tag{C9}$$

We do not consider here the behavior of n_2 for frequencies $\omega > 2\Delta + T_*$.

APPENDIX D: NORMALIZATION EQUATION

We derive here an explicit expression for the coefficients I_i ($i = 0, 1, 2$) entering Eq. (45) for the normalization constant b_0 . To find those coefficients, we substitute Eq. (44)

into Eq. (43) and divide the result by $(2\Delta)^3/(1 + \tau_l/\tau_0^{\text{PB}})$. From the term containing n_T we find

$$I_0 = \frac{1}{(2\Delta)^3} \int_{2\Delta} d\omega \omega^2 n_T(\omega, T_B) \simeq \frac{T_B}{2\Delta} e^{-2\Delta/T_B}. \tag{D1}$$

To find I_2 , we collect together the terms quadratic in f , switch the integration order between ω and E , and change variables from ω to $E' = \omega - E$; we obtain

$$\begin{aligned}
I_2 &= \frac{1}{b_0^2 \pi \Delta (2\Delta)^3} \int_{\Delta} dE \int_{\Delta} dE' (E + E')^2 \rho(E) \\
&\quad \times U^+(E, E') f(E) f(E'). \tag{D2}
\end{aligned}$$

The presence of the two distribution functions implies that the main contributions to the integrals come from regions close to Δ , and using approximations similar to those used in Eq. (41), we arrive at

$$I_2 \simeq \frac{(2.1)^2}{\pi} \frac{T_*}{2\Delta}. \tag{D3}$$

Finally, considering the n_1 term, we get

$$\begin{aligned}
I_1 &= \frac{1}{b_0 \pi \Delta (2\Delta)^3} \int_{\Delta} dE \int_{2\Delta} d\omega \omega^2 \rho(E) \\
&\quad \times U^-(E, E + \omega) f(E + \omega). \tag{D4}
\end{aligned}$$

Here we have to consider separately various regimes. For high phonon temperature and low photon number, $T_B^* \lesssim T_B \ll T_*$, the distribution function takes the Boltzmann form $f(E) = b_T e^{-E/T_B}$ above energy $E_* \lesssim 2\Delta < 3\Delta$ (see Sec. III B), and we have

$$I_1 \simeq \frac{1}{\sqrt{2\pi}} \frac{b_T}{b_0} \left(\frac{T_B}{2\Delta} \right)^{3/2} e^{-3\Delta/T_B}, \tag{D5}$$

where

$$\frac{b_T}{b_0} \simeq \frac{3}{2^{5/6} \sqrt{\pi}} \left(\frac{T_B}{T_*} \right)^{1/4} e^{\Delta/T_B} e^{(2/3)(T_*/T_B)^{3/2}}. \tag{D6}$$

With these expressions, using $(T_*/\Delta)^3 \lesssim T_B/\Delta$, we can rewrite the condition for the normalization constant b_0 to give the thermal-equilibrium density as $0.16(\tau_l/\tau_0^{\text{PB}})^2 (T_B/\Delta)^2 e^{-2\Delta/3T_B} < 1$; even at the relatively high temperature $T_B = 0.3T_c$, this condition becomes $10^{-4}(\tau_l/\tau_0^{\text{PB}})^2 < 1$, showing that in this regime deviations from the thermal-equilibrium density are possible only if τ_l exceeds τ_0^{PB} by at least a few orders of magnitude. We do not pursue the analysis of this large- τ_l limit here, as we focus on the experimentally relevant case of aluminum films in which τ_l is comparable to τ_0^{PB} . However, the large- τ_l regime could be relevant for other materials, such as niobium.

For low phonon temperature and high photon number, $T_B \ll T_B^*$, we have $E_* \gtrsim 2\Delta$, so we need to distinguish between $E_* < 3\Delta$ and $E_* > 3\Delta$. In the former case, Eq. (D5) still holds, but now

$$\frac{b_T}{b_0} \simeq \frac{3^{3/2}}{2^{1/3}\sqrt{5\pi}} \sqrt{\frac{35}{64}} \left(\frac{T_B}{\Delta}\right)^{1/2} \left(\frac{T_*}{\Delta}\right)^{-1} \times e^{\Delta/T_B} e^{(3/5)(\tilde{T}_*/T_B)^{5/3}}. \quad (\text{D7})$$

Using this expression, one can check that the condition for b_0 to give the thermal-equilibrium density is easily violated, due to the last exponential factor in Eq. (D7) being dominant and large in the regime $T_B/\Delta \ll (T_*/\Delta)^3$ (the violation occurs unless τ_l/τ_0 is small compared with the inverse of that exponential factor). Similarly, in the case $E_* > 3\Delta$, we find again that the density generically deviates from the thermal-equilibrium density. In this case we have

$$I_1 = \frac{3^{3/2}}{2^{7/3}5\pi\sqrt{7}} \left(\frac{T_*}{\Delta}\right)^5 \exp\left[-\sqrt{\frac{14}{5}} \left(\frac{\Delta}{T_*}\right)^3\right], \quad (\text{D8})$$

and in the ratio $I_1^2/(I_0I_2)$ the exponential factor $e^{2\Delta/T_B}$ from I_0 dominates over the exponential in I_1 . Note that despite the similarity, the coefficient I_1 and hence the value of b_0 in the two cases are different. Also, although we include the case $E_* < 3\Delta$ for completeness, it has limited relevance, since the inequality holds if $(T_*/\Delta)^3 < 2^{3/2}\sqrt{35/64}(T_B/\Delta)$, and at the same time we require $T_B/\Delta \ll (T_*/\Delta)^3$.

To summarize, we find that for high phonon temperature and low photon number the quasiparticle density is the same as in thermal equilibrium and the term linear in b_0 in Eq. (45) can be ignored. Conversely, at low phonon temperature and high photon number the constant term can be ignored. The relationship to the generalized Rothwarf-Taylor equation can be found by restoring all prefactors; in practice, this amounts to expressing b_0 in terms of N_{QP} using Eq. (41), multiplying the left-hand side of Eq. (45) by $4\rho_F(2\Delta/T_c)^3\pi\Delta/\bar{\tau}_0$, and equating the result to dN_{QP}/dt . In this procedure, we can use Eq. (D8) for I_1 ; in this way, the crossover between the two regimes is correctly identified up to numerical factors of order unity.

APPENDIX E: PHOTON-NUMBER-DEPENDENT CORRECTIONS IN THE GENERALIZED RT MODEL

In the discussion of the generalized RT model in Sec. IV A, we limit our considerations to the leading order in the parameter $T_*/\Delta \lesssim 1$. However, corrections in powers of $\varepsilon \equiv T_*/\Delta$ can be taken into account, as we now show. We begin by evaluating corrections to the expression for the quasiparticle density, Eq. (41).

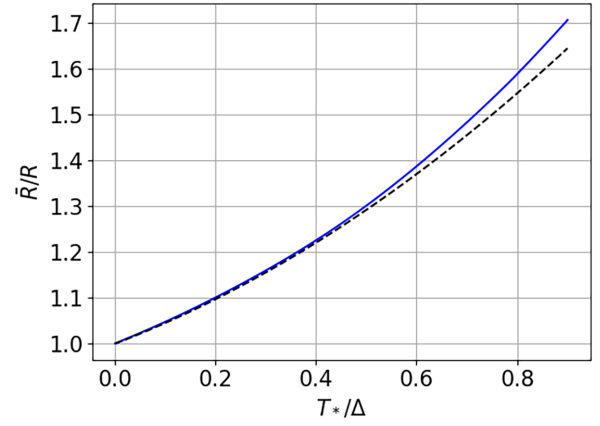


FIG. 8. Numerically calculated recombination coefficient (solid blue line) for the distributions derived in Sec. III (for $T_B = 0$), in the unit of the (zeroth-order) recombination coefficient R defined in Eq. (49), and the analytical approximation (dashed black line), Eq. (E2).

In the integral there, we make the change of variables $E = \Delta(1 + \varepsilon x)$ and express the density of states as $\rho(E) \simeq \sqrt{\Delta/2T_*x} (1 + 3\varepsilon x/4 - 5(\varepsilon x)^2/32)$. Defining $a_\beta = \int_0 dx x^\beta f(x)/b_0$, we find

$$N_{\text{QP}} \simeq 2\rho_F\sqrt{2T_*\Delta}b_0 \left(a_{-1/2} + \frac{3}{4}a_{1/2}\varepsilon - \frac{5}{32}a_{3/2}\varepsilon^2 \right). \quad (\text{E1})$$

The a_β factors can be estimated numerically; they have the values $a_{-1/2} \simeq 2.1$, $a_{1/2} \simeq 0.88$, and $a_{3/2} \simeq 0.77$.

The same procedure can be applied to the evaluation of I_2 in Eq. (D2) by expanding in the integral the energy-dependent factors multiplying the two distribution functions. By comparing the result with the square of Eq. (E1), we find that the recombination term in Eq. (47) can be written as $\bar{R}N_{\text{QP}}^2$, with

$$\frac{\bar{R}}{R} = 1 + \frac{a_{1/2}}{a_{-1/2}}\varepsilon + \left[\frac{5}{4} \frac{a_{3/2}}{a_{-1/2}} - \frac{3}{4} \left(\frac{a_{1/2}}{a_{-1/2}} \right)^2 \right] \varepsilon^2 \quad (\text{E2})$$

and R defined in Eq. (49). In Fig. 8 we show that this second-order-in- ε expression gives a reasonable approximation for the recombination coefficient even for T_* close to Δ .

Additional corrections originate from our taking into account the dependence on ω of the phonon pair-breaking lifetime $\tau_{\text{PB}}^{\text{phon}}(\omega)$, Eq. (A2), which we previously ignored. In the expression for the phonon distribution function, Eq. (C6), this amounts to the substitution $\zeta \rightarrow \zeta(\omega)$, where the energy-dependent phonon trapping factor is

$$\zeta(\omega) = 1 + \tau_l/\tau_{\text{PB}}^{\text{phon}}(\omega). \quad (\text{E3})$$

We also need to modify Eq. (43) by multiplying the distribution function $n(\omega)$ by $\tau_0^{\text{PB}}/\tau_{\text{PB}}^{\text{phon}}(\omega)$. Inserting the thus-corrected Eq. (C6) into the modified Eq. (43), we find that the two integrals I_0 and I_1 for the generation terms are modified by inserting in the integrands of Eqs. (D1) and (D4) a factor $\tau_0^{\text{PB}}\zeta/\tau_{\text{PB}}^{\text{phon}}(\omega)\zeta(\omega)$, while in the integrand for the generation term I_2 , Eq. (D2), we must include the factor $\zeta/\zeta(E+E')$. Since in the relevant regime ($T_B \ll T_B^*$) I_1 has stronger-than-exponential dependence on T_*/Δ , see Eq. (D8), we do not pursue the calculation of weak corrections proportional to $\varepsilon^{9/5}$ [the main correction to the function $G(x)$ originates from the linear term in Eq. (E1) for N_{QP} , so the right-hand side of Eq. (51) should be multiplied by $1 - (3a_{1/2}/4a_{-1/2})\varepsilon$]. Similarly, we ignore the small corrections in T_B/Δ that would be introduced to the leftmost expression in Eq. (D1). For I_2 , we limit ourselves to terms linear in ε ; at this order we find that the coefficient of the linear term in Eq. (E2) should be multiplied by $(1 + \tau_l/2\tau_0^{\text{PB}})/(1 + \tau_l/\tau_0^{\text{PB}})$. As a function of τ_l , this factor varies between 1 and 1/2, so the finite thermalization time can weaken the dependence of the recombination coefficient \bar{R} on T_*/Δ , but it does not change its increase with this parameter. Therefore, in the high-phonon-temperature regime, $T_B \gtrsim T_B^*$, in which the I_1 term can be ignored, this increase implies a decrease of quasiparticle number with increasing photon number.

APPENDIX F: PARAMETERS FOR COMPARISON WITH EXPERIMENT

We discuss here our estimates for the parameters used in the comparison with the experiment reported in Ref. [13] (see Table II in Sec. V). The kinetic inductance fraction α and the zero-temperature gap Δ_0 are obtained by our fitting the measured internal quality factor for temperatures $T > 0.25$ K and the lowest readout power, $P_{\text{read}} = -100$ dBm, to the thermal-equilibrium expression [31]

$$Q_i = \frac{\pi}{4\alpha \sinh(x)K_0(x)} \exp\left(\frac{\Delta_T}{T}\right), \quad (\text{F1})$$

where $x = \omega_0/2T$ and K_0 is the zeroth-order modified Bessel function. A least-squares fit gives $\alpha \simeq 0.13$ and $\Delta_0 \simeq 189$ μeV . The assumption of thermal equilibrium for the quasiparticles is justified, since the estimated T_* is comparable to ω_0 (see Table III).

The kinetic inductance fraction can be estimated on the basis of the geometry of the resonator using Eqs. (8) and (46) in Ref. [41] (in the latter equation, the penetration depth can be estimated using the measured value of resistivity); this yields $\alpha = 0.07$, which is of the same order as the value obtained from the fit. In Ref. [13] a smaller value for Δ_0 is given, estimated by measuring the critical temperature and using the BCS relation for the ratio Δ_0/T_c ; our estimate agrees with previous findings of a

higher ratio in thin aluminum films [42]. To estimate $c_{\text{phot}}^{\text{QP}}$ using Eq. (15), we follow Ref. [13] and assume the volume occupied by the quasiparticles to be twice the central strip volume, $V = 2 \times 1770$ μm^3 , to account for quasiparticles in the ground plane, and take $\rho_F = 1.74 \times 10^4/\mu\text{eV}$ μm^3 . Then for thin-film resonators we use $Q' = \pi \Delta_0/\alpha\omega_0$, as can be seen by replacement of $\sigma_1 \rightarrow \sigma_N$ in the central expression in Eq. (57).

-
- [1] A. F. G. Wyatt, V. M. Dmitriev, W. S. Moore, and F. W. Sheard, Microwave-Enhanced Critical Supercurrents in Constricted Tin Films, *Phys. Rev. Lett.* **16**, 1166 (1966).
 - [2] A. H. Dayem and J. J. Wiegand, Behavior of thin-film superconducting bridges in a microwave field, *Phys. Rev.* **155**, 419 (1967).
 - [3] G. M. Eliashberg, Film superconductivity stimulated by a high-frequency field, *JETP Lett.* **11**, 114 (1970).
 - [4] J. E. Mooij, in *Nonequilibrium Superconductivity, Phonons, and Kapitza Boundaries*, edited by K. E. Gray (Springer US, Boston, MA, 1981), p. 191.
 - [5] T. Klapwijk and P. de Visser, The discovery, disappearance and re-emergence of radiation-stimulated superconductivity, *Ann. Phys. (N. Y.)* **417**, 168104 (2020).
 - [6] P. K. Day, H. G. LeDuc, B. A. Mazin, A. Vayonakis, and J. Zmuidzinas, A broadband superconducting detector suitable for use in large arrays, *Nature* **425**, 817 (2003).
 - [7] C. M. Natarajan, M. G. Tanner, and R. H. Hadfield, Superconducting nanowire single-photon detectors: physics and applications, *Supercond. Sci. Technol.* **25**, 063001 (2012).
 - [8] G. Catelani and J. P. Pekola, Using materials for quasiparticle engineering, *Mater. Quantum Technol.* **2**, 013001 (2022).
 - [9] J.-J. Chang and D. J. Scalapino, Kinetic-equation approach to nonequilibrium superconductivity, *Phys. Rev. B* **15**, 2651 (1977).
 - [10] B. I. Ivlev, S. G. Lisitsyn, and G. M. Eliashberg, Nonequilibrium excitations in superconductors in high-frequency fields, *J. Low Temp. Phys.* **10**, 449 (1973).
 - [11] G. Catelani and D. M. Basko, Non-equilibrium quasiparticles in superconducting circuits: Photons vs. phonons, *SciPost Phys.* **6**, 13 (2019).
 - [12] D. J. Goldie and S. Withington, Non-equilibrium superconductivity in quantum-sensing superconducting resonators, *Supercond. Sci. Technol.* **26**, 015004 (2012).
 - [13] P. J. de Visser, D. J. Goldie, P. Diener, S. Withington, J. J. A. Baselmans, and T. M. Klapwijk, Evidence of a Nonequilibrium Distribution of Quasiparticles in the Microwave Response of a Superconducting Aluminum Resonator, *Phys. Rev. Lett.* **112**, 047004 (2014).
 - [14] J. Gao, J. Zmuidzinas, A. Vayonakis, P. Day, B. Mazin, and H. LeDuc, Equivalence of the effects on the complex conductivity of superconductor due to temperature change and external pair breaking, *J. Low. Temp. Phys.* **151**, 557 (2008).
 - [15] F. Valenti, F. Henriques, G. Catelani, N. Maleeva, L. Grünhaupt, U. von Lüpke, S. T. Skacel, P. Winkel, A. Bilmes, A. V. Ustinov, J. Goupy, M. Calvo, A. Benoît,

- F. Levy-Bertrand, A. Monfardini, and I. M. Pop, Interplay between Kinetic Inductance, Nonlinearity, and Quasiparticle Dynamics in Granular Aluminum Microwave Kinetic Inductance Detectors, *Phys. Rev. Appl.* **11**, 054087 (2019).
- [16] E. M. Levenson-Falk, F. Kos, R. Vijay, L. Glazman, and I. Siddiqi, Single-Quasiparticle Trapping in Aluminum Nanobridge Josephson Junctions, *Phys. Rev. Lett.* **112**, 047002 (2014).
- [17] L. Grünhaupt, N. Maleeva, S. T. Skacel, M. Calvo, F. Levy-Bertrand, A. V. Ustinov, H. Rotzinger, A. Monfardini, G. Catelani, and I. M. Pop, Loss Mechanisms and Quasiparticle Dynamics in Superconducting Microwave Resonators Made of Thin-Film Granular Aluminum, *Phys. Rev. Lett.* **121**, 117001 (2018).
- [18] G. M. Eliashberg, Inelastic electron collisions and nonequilibrium states in superconductors, *Sov. Phys. JETP* **34**, 668 (1972).
- [19] J.-J. Chang and D. J. Scalapino, Nonequilibrium superconductivity, *J. Low Temp. Phys.* **31**, 1 (1978).
- [20] J. Bardeen, L. N. Cooper, and J. R. Schrieffer, Theory of superconductivity, *Phys. Rev.* **108**, 1175 (1957).
- [21] S. B. Kaplan, C. C. Chi, D. N. Langenberg, J. J. Chang, S. Jafarey, and D. J. Scalapino, Quasiparticle and phonon lifetimes in superconductors, *Phys. Rev. B* **14**, 4854 (1976).
- [22] A. Zehnder, Response of superconductive films to localized energy deposition, *Phys. Rev. B* **52**, 12858 (1995).
- [23] To check this expression, we note that the power P_{abs} absorbed by the quasiparticles can be calculated by multiplying St^{phot} , Eq. (14), by $4\rho_F V E \rho(E)$ and integrating the resulting expression over E ; for $\bar{n} \gg 1$, comparing the result with Eq. (54) for σ_1 , we find $P_{\text{abs}} = 2\bar{n}\omega_0^2 c_{\text{phot}}^{\text{QP}} \sigma_1 / \sigma_N \delta$. The inverse quality factor is by definition $1/Q = P_{\text{abs}} / \omega_0 \mathcal{E}$, with $\mathcal{E} = \bar{n}\omega_0$ the energy stored in the resonator [see Eq. (59)]. Using that in the normal state $\sigma_1 = \sigma_N$, we arrive at Eq. (15).
- [24] A. G. Kozorezov, J. K. Wigmore, A. Peacock, R. den Hartog, D. Martin, G. Brammertz, P. Verhoeve, and N. Rando, Evidence for an excited nonequilibrium quasiparticle distribution in superconducting tunnel junctions resulting from energy accumulation via sequential tunneling, *Phys. Rev. B* **69**, 184506 (2004).
- [25] In contrast to our procedure, in which the BCS density of states, Eq. (3), is kept unaltered, some authors introduce a broadened density of states and a cutoff using a Heaviside function [12,43]. This approach can be problematic; for example, in our understanding, the discretized version of the photon integral used in Ref. [43] violates the conservation of the number of quasiparticles. With our approach, introducing a broadening and a cutoff is not necessary, and terms that conserve the number of quasiparticles in Eq. (1) also conserve the number of quasiparticles in the discretized version..
- [26] S. B. Kaplan, Acoustic matching of superconducting films to substrates, *J. Low Temp Phys.* **37**, 343 (1979).
- [27] W. Eisenmenger, K. Laßmann, H. J. Trumpp, and R. Krauß, Quasiparticle recombination and 2Δ -phonon-trapping in superconducting tunneling junctions, *Appl. Phys.* **11**, 307 (1976).
- [28] A. Rothwarf and B. N. Taylor, Measurement of Recombination Lifetimes in Superconductors, *Phys. Rev. Lett.* **19**, 27 (1967).
- [29] G. Catelani, L. I. Glazman, and K. E. Nagaev, Effect of quasiparticles injection on the ac response of a superconductor, *Phys. Rev. B* **82**, 134502 (2010).
- [30] D. V. Nguyen, G. Catelani, and D. M. Basko, Dissipation in a superconducting artificial atom due to a single nonequilibrium quasiparticle, *Phys. Rev. B* **96**, 214508 (2017).
- [31] J. Gao, Ph.D. thesis, California Institute of Technology, 2008.
- [32] D. M. Pozar, *Microwave Engineering* (John Wiley & Sons Inc, Hoboken, NJ, 2012), fourth ed.
- [33] G. Catelani, R. J. Schoelkopf, M. H. Devoret, and L. I. Glazman, Relaxation and frequency shifts induced by quasiparticles in superconducting qubits, *Phys. Rev. B* **84**, 064517 (2011).
- [34] We stress here that in discretizing the kinetic equations attention must be paid to avoiding the introduction of an unphysical quasiparticle source (see Ref. [25]); in numerical calculations this would cause saturation of the quality factor to levels lower than our estimates provide.
- [35] P. Macha, S. H. W. van der Ploeg, G. Oelsner, E. Il'ichev, H.-G. Meyer, S. Wünsch, and M. Siegel, Losses in coplanar waveguide resonators at millikelvin temperatures, *Appl. Phys. Lett.* **96**, 062503 (2010).
- [36] C. C. Chi and J. Clarke, Quasiparticle branch mixing rates in superconducting aluminum, *Phys. Rev. B* **19**, 4495 (1979).
- [37] A. V. Semenov, I. A. Devyatov, P. J. de Visser, and T. M. Klapwijk, Coherent Excited States in Superconductors due to a Microwave Field, *Phys. Rev. Lett.* **117**, 047002 (2016).
- [38] M. Houzet, K. Serniak, G. Catelani, M. H. Devoret, and L. I. Glazman, Photon-Assisted Charge-Parity Jumps in a Superconducting Qubit, *Phys. Rev. Lett.* **123**, 107704 (2019).
- [39] L. I. Glazman and G. Catelani, Bogoliubov quasiparticles in superconducting qubits, *SciPost Phys. Lect. Notes* **31** (2021)
- [40] A. G. Kozorezov, J. K. Wigmore, G. Brammertz, and A. Peacock, The role of phonons in establishing a nonequilibrium quasiparticle state in small gap multiple tunnelling superconducting tunnel junctions, *Physica Status Solidi (c)* **1**, 2816 (2004).
- [41] J. R. Clem, Inductances and attenuation constant for a thin-film superconducting coplanar waveguide resonator, *J. Appl. Phys.* **113**, 013910 (2013).
- [42] P. Chubov, V. Eremenko, and Y. A. Pilipenko, Dependence of the critical temperature and energy gap on the thickness of superconducting aluminum films, *Sov. Phys. JETP* **28**, 389 (1969).
- [43] T. Guruswamy, Ph.D. thesis, Apollo—University of Cambridge Repository, 2018.